Nonequilibrium Dynmical Mean Field Theory based on the Non-Crossing Approximation

Hristiana Atanasova

March 29, 2018

Contents

1 Introduction **3**

2 Theoretical concepts **3**
- 2.1 Hubbard model . . . 3
- 2.2 Overview of equilibrium dynamical mean field theory . . . 3
- 2.3 Nonequilibrium DMFT formalism . . . 6
- 2.4 Solving the Anderson impurity model . . . 7
  - 2.4.1 Physical observables and the contour idea . . . 7
  - 2.4.2 Green's function computation within the non-crossing approximation . . . 9
  - 2.4.3 Properties of the Green's functions . . . 13
- 2.5 Time-dependent electric fields . . . 14
- 2.6 Dissipative systems . . . 15

3 Implementation **17**
- 3.1 Bethe lattice . . . 17
- 3.2 Initial setup . . . 17
- 3.3 Dissipation . . . 17
- 3.4 Physical observables . . . 18
- 3.5 Numerical implementation . . . 18

4 Results **18**
- 4.1 Equilibrium properties . . . 18
- 4.2 Magnetic relaxation in a periodically driven Hubbard model . . . 19
  - 4.2.1 Undriven magnetic melting . . . 19
  - 4.2.2 Magnetic melting in resonant driven lattices . . . 20
- 4.3 Energy dissipation in a periodically driven system . . . 21
  - 4.3.1 Unphysical Bethe lattice . . . 21
  - 4.3.2 Physical lattice structure . . . 32

1 Introduction

2 Theoretical concepts

2.1 Hubbard model

During its 50-year old history the Hubbard model has, despite its simplicity, become the most famous model for the study of strongly correlated materials. It was introduced by Hubbard, Gutzwiller and Kanamori (citation) in 1963 for the study of correlated d-electrons in transition metals, showing a bahaviour that arises from localization as well as delocalization effects. The Hamiltonian in second quantization describes a collection of single level atoms associated with Wannier orbitals centered at each site of the crystal lattice and is given by

$$H_{Hubbard} = -\sum_{\langle i,j\rangle,\sigma}^{N} v_{ij} d_{i\sigma}^{\dagger} d_{j\sigma} + \epsilon_0 \sum_{i,\sigma}^{N} d_{i\sigma}^{\dagger} d_{i\sigma} + U \sum_{i}^{N} d_{i\uparrow}^{\dagger} d_{i\uparrow} d_{i\downarrow}^{\dagger} d_{i\downarrow},$$

where N is the number of lattice sites and the operator $d_{i\sigma}^{\dagger}[d_{i\sigma}]$ creates[destroys] an electron with spin σ at the lattice site with coordinate $\mathbf{R}_{i(j)}$. The first term describes the amplitude for an electron to hop between site i and j and its magnitude depends on the overlap between the orbitals. The kinetic energy term is diagonalized in a single particle basis of Bloch's wavefunctions

$$\epsilon_k = \sum_j v_{ij} exp^{ik(R_i - R_j)}$$

known as a single tight-binding band. Since the hopping amplitude decreases strongly with increasing site distance, we take only nearest neighbour hopping into account. The second term is the on-site energy and the last one the Coulomb repulsion of two electrons with opposite spin occupying the same orbital. Because the bands are assumed to be strongly localized at the lattice sites, electron interactions between different sites are neglected.

The Hubbard Model captures the competition between two key energy scales: the kinetic energy and the Coulomb repulsion. In the absence of hopping the model reduces to the four atomic states $|0\rangle, |\uparrow\rangle, |\downarrow\rangle$ and $|\uparrow\downarrow\rangle$ with energies $0, \epsilon_0, U + 2\epsilon_0$. A system at half filling, correspoding to $\epsilon_0 = -\frac{U}{2}$, and the limiting cases regarding the Coulomb interaction are often cosidered to gain further insight to the model.

- In the limit of $U \to 0$ the model reduces to a single-band tight-binding model representing a metal
- For $U \to \infty$ the electrons are localizes and the systems becomes a so-called Mott-insulator

The crossover between those limits, when the kinetic energy and the Coulomb repulsion are competing, opens up a variety of new physical phenomena and is essential for the understanding of strongly correlated materials.

- TODO: add schmatic representation of Hubbard model and atomic energies at half filling

2.2 Overview of equilibrium dynamical mean field theory

Dynamical Mean Field Theory (DMFT) has become a powerful method when it comes to the study of many body systems involving strong electronic correlations in as well as out of equilibrium. We will start with a

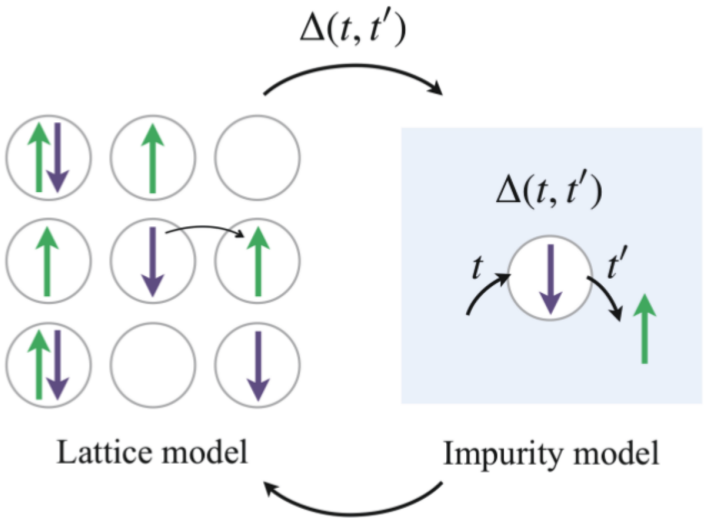

Figure 1: Schematic representation of the DMFT formalism, where the lattice model is mapped onto an impurity problem. $\Delta(t,t')$ is the hybridization between the single site and the bath and $\Sigma(t,t')$ is the self-energy.

brief overview of the DMFT equations in equilibirum and extend them to the nonequilibrium analogue in the next chapter. The idea of DMFT is to solve the lattice problem with many degrees of freedom by mapping it to an impurity problem consisting of a single correlated site embedded in an uncorrelated bath, formed by the residual sites of the lattice. The hybridization between the impurity and the bath is the dynamical mean field $\Delta(t,t')$. It resembles the exchange of particles with the rest of the lattice and must be determined self consistently as a functional of the lattice Greens function $G_{ij}(t,t')$. The key approximation is the local nature of the lattice self energy

$$\Sigma_{ij}(t,t') \backsimeq \delta_{ij}\Sigma_{ii}(t,t') \tag{1}$$

that justifies the mapping.

Since in equilibrium all functions depend only on time-differences, they are represented in frequency space by their Fourier transforms. As mentioned in the last chapter, the simplest model for the description of strongly correlated systems is the single band Hubbard model representing a collection of single orbital atoms placed at the nodes of a crystal lattice. For a system at half-filling the Hamiltonian reads as

$$H_{Hubbard} = -\sum_{\langle i,j\rangle,\sigma} v_{ij} d^{\dagger}_{i\sigma} d_{j\sigma} + \sum_{i} U(d^{\dagger}_{i\uparrow}d_{i\uparrow} - \frac{1}{2})(d^{\dagger}_{i\downarrow}d_{i\downarrow} - \frac{1}{2}).$$

With the approximation that the lattice self energy is local in space the local Greens function

$$\mathrm{G}^{\sigma}_{\mathrm{ii}}(\mathrm{t}-\mathrm{t}') = -\mathrm{i}\langle \mathcal{T}\mathrm{d}_{\mathrm{i}\sigma}(\mathrm{t})\mathrm{d}^{\dagger}_{\mathrm{i}\sigma}(\mathrm{t}')\rangle,$$

where $\mathcal{T}$ is the time ordering operator, can be computed from an effective impurity model described by the action

$$S_i = i\int_c dt U n_\uparrow(t) n_\downarrow(t) - i\sum_\sigma \int_c dt dt' d^\dagger_\sigma(t)\Delta_i(t-t')d_\sigma(t'). \tag{2}$$

At time t' an electron hops from the fictious bath to the dot and goes back to the bath at time t, where $\Delta_i(t-t')$ is the amplitude for this process to happen. Whenever two electrons occupy the same site simultaniously this results in an energy cost U, hence the action captures the fluctuation between the four atomic states $|0\rangle, |\uparrow\rangle, |\downarrow\rangle$ and $|\uparrow\downarrow\rangle$. It is important to see that DMFT is a mean field only in terms of spacial fluctuations, which are freezed, but it takes account of all local temporal fluctuations, hence the name "dynamical". From here on the spin index will be supressed for simplicity.

To solve the impurity problem means to compute the impurity Greens's functions, which can be challenging, but still feasible and is considered here in Chapter 2.6. Once the impurity Green's function is obtained, the impurity self-energy is extracted from the Dyson equation

$$G^{-1}_{ii}(\omega) = \omega + \mu - \Delta_i(\omega) - \Sigma^{imp}_{ii}(\omega),$$

where $\mathcal{G}_0^{-1}(\omega) = \omega + \mu - \Delta_i(\omega)$ is the non-interacting Green's function, known as the "Weiss function". The approximation for the self-energy 1 is then used to obtain the lattice Greens function

$$G^{-1}_{ij}(\omega) = \delta_{ij}[\omega + \mu - \Sigma^{imp}_{ii}(\omega)] - v_{ij}.$$

In real space this means that all non-local components of the lattice self-energy $\Sigma_{ij}(\omega)$ are neglected and the local component corresponds to $\Sigma^{imp}_{ii}(\omega)$. For a translationally invariant system ($\Sigma_{ii}(\omega) \equiv \Sigma(\omega)$) one averages over the whole Brillouin zone to get the on-site component of the lattice Green function, which is referred to as the self-consistency condition

$$G_{ii}(\omega) = \frac{1}{N}\sum_k G_k(\omega) = \frac{1}{N}\sum_k \frac{1}{\omega + \mu + \Sigma(\omega) - \epsilon_k},$$

with $G_k(\omega)$ the momentum resolved Greens function, N the number of lattice sites and ϵ_k the dispersion relation of the non-interacting tight binding band

$$\epsilon_k = \sum_j v_{ij} exp^{ik(R_i - R_j)}.$$

Instead of performing the k-summation one can integrate over the local, non-interacting Density of states $\mathrm{D}(\epsilon) = \frac{1}{\mathrm{N}}\sum_{\mathrm{k}} \delta(\epsilon - \epsilon_{\mathrm{k}})$

$$G_{ii}(\omega) = \int d\epsilon \frac{D(\epsilon)}{\omega + \mu + \Sigma(\omega) - \epsilon}.$$

The self-consistency condition relates for each frequency ω the dynamical mean field to the local lattice Green's function. This functional relation G[Δ] provides a closed set of equations to determine $\Delta(\omega)$ and G(ω). This can be done by an iterative procedure that does not depend on the initial guess for $\Delta(\omega)$. In a DMFT cycle the lattice model is mapped onto an auxiliary Anderson impurity model (AIM), which is described in Chapter 2.4. The methods for solving the auxiliary problem are called impurity solvers, a real-time impurity solver based on the strong-coupling expansion is used in this thesis. With the impurity solver the Green's function and a the self-energy are calculated, which are used to update the hybridization

function. The hybridization function is then used to start a new DMFT-cycle. This procedure repeats until a convergence criterium is reached.

Metzner and Vollhart showed that in the limit of infinite nearest neighbours, known as the coordination number Z, DMFT becomes exact if the hopping is rescaled properly

$$v_{ij} = \frac{v_{ij}^*}{\sqrt{Z}},$$

with a constant v_{ij}^* ensuring that the kinetic energy remains finite and the competition between kinetic and potential energy is preserved. The approximation for the self-energy 1 then holds exactly

$$\lim_{Z\to\infty} \Sigma_{ij}(t,t') = \delta_{ij}\Sigma_{ii}(t,t').$$

Several proofs for this exist including a linked cluster expansion around the atomic limit or a cavity method approach. Anyways it is quite intuitive that if the number of nearest neighbours is very large, spatial fluctuations become negligible. Other exact solutions are given in the noninteracting limit ($U = 0$), where the local lattice Green's function reduces to $G_{ii}(\omega) = \mathcal{G}_0^{-1}(\omega)$, and in the atomic limit ($v_{ij} = 0$), where the system is a collection of disconnected sites.

- TODO: own schematic representation of DMFT mapping

2.3 Nonequilibrium DMFT formalism

To capture non-equilibrium physics in time-dependent systems (e.g. an electric-field driven lattice system) all objects within the set of DMFT equations need to incorporate the overall temporal evolution of the system as well as quantum fluctuations. Analogous to the equilibirum case, in the limit $Z \to \infty$ the self energy is local in space

$$\Sigma_{ij}(t,t') = \delta_{ij}\Sigma_i(t,t')$$

and is used to obtain the contour-ordered lattice Green's function $G_{ij}(t,t') = -i\langle \mathcal{T} d_i(t) d_j^\dagger(t')\rangle$ from the Dyson equation

$$G_{ij}^{-1}(t,t') = (G_0^{-1})_{ij}(t,t') - \delta_{ij}\Sigma_{ii}(t,t')$$

with the non-interacting lattice Green's function $(G_0^{-1})_{ij}(t,t')$. As for an equilibrium system the effective impurity action needs to be solved

$$S_i = i\int_c dt U n_\uparrow(t) n_\downarrow(t) - i\sum_\sigma \int_c dt dt' d_\sigma^\dagger(t)\Delta_i(t,t') d_\sigma(t')$$

as part of an iterative procedure until the impurity Green's function corresponds to the local lattice Green's function. Besides depending on two times the equations for non-equilibirum DMFT look formally identical to the ones presented in the previous chapter. The conceptual difference is the non-markovian structure with the self-energy as the memory kernel.

2.4 Solving the Anderson impurity model

It was first shown by Georges ans Kotliar in 1992 that the Hubbard model in infinite Z is equivalent to the Anderson impurity model (AIM)

$$H_{imp} = H_D + H_B + H_{hyb}, \tag{3}$$

with the dot-Hamiltonian

$$H_D = \sum_{\sigma\epsilon\uparrow,\downarrow} \varepsilon_\sigma d_\sigma^\dagger d_\sigma + U d_\uparrow^\dagger d_\uparrow d_\downarrow^\dagger d_\downarrow,$$

where ε_σ are the on-site energy levels and U is the interaction between electrons having opposite spins. $\mathrm{H_{imp}}$ can in general incorporate a time-dependence, but for now we will consider only time-independent impurity models. There are four possible dot eigenstates $|0\rangle, |\uparrow\rangle, |\downarrow\rangle, |\uparrow\downarrow\rangle$ corresponding to the dot being empty or occupied by either one or two electrons. The non-interacting bath Hamiltonian has the form

$$H_B = \sum_{\sigma,k} \varepsilon_k b_k^\dagger b_k$$

and the coupling between dot and bath is given through the Hybridization

$$H_{hyb} = \sum_{\sigma,k} (v_{\sigma k} b_k^\dagger d_\sigma + v_{\sigma k}^* d_\sigma^\dagger b_k),$$

which describes processes in which electrons are hopping from the bath to the dot and vice versa. The AIM 3 is the hamiltonian representation of the action 2, which can be seen by integrating out the quadratic bath contribution $b_k^\dagger b_k$. This auxiliary model is solved self-consistently as part of the DMFT cycle.

2.4.1 Physical observables and the contour idea

Expectation values of observables $\langle O(t)\rangle$, where $\langle\cdots\rangle$ denotes a quantum and a statistical average, can be related to experimental measurements. If the measurement is time dependent, a framework which tracks the temporal evolution of the statistical ensemble is desirable. Our main goal is to calculate the time dependent correlation of these observables, such as

$$\langle O(t)O(t')\rangle.$$

Knowing all correlations of all observables, would fully describe the system. In second quantization these correlations come in pairs of creation and annihilation operators, which are called Green's functions. A n-particle Green's function with the creation and annihilation operators $d(t), d^\dagger(t')$ is given by

$$G_n(t_1,...,t_n;{t'}_n,...,t'_1) = (-i)^n \langle d(t_1)...d(t_n)d^\dagger(t'_n)...d^\dagger(t'_1)\rangle$$

and the operators obey the commutation [anticommutation] relations for bosons [fermions]

$$[d(i),d(j)]_{-[+]} = \left[d^\dagger(i),d^\dagger(j)\right]_{-[+]} = 0,$$

$$\left[d(i),d^\dagger(j)\right]_{-[+]} = \delta_{ij}.$$

We are interested in the calculation of one-particle correlation functions like $G^{>}(t,t') = -i\langle \mathrm{d(t)d^{\dagger}(t')}\rangle$ and $G^{<}(t,t') = i\langle \mathrm{d^{\dagger}(t')d(t)}\rangle$ from which information about physical properties of the system, like the density of single particle excitations, can be extracted.

The expectation value $\langle \cdots \rangle$ of an operator O at time t is given by

$$\langle O(t)\rangle = tr\left(\rho U^{\dagger}(t_0,t)\hat{O}U(t,t_0)\right),$$

with the time evolution operator $U(t,t_0)$, which propagates a quantum system in time. The initial density matrix ρ, that can be factorized into the dot ρ_D and the bath ρ_B density matrix, since the dot is initially decoupled from the bath. If one reads the trace from left to the right, it could be interpreted as oriented contour depicted in Fig. ...: States are propagated from time t_0 to t, then an operator acts at time t, after which the states are propagated back to t_0. The forward [backward] propagation is represented by $U(t,t_0)$ $[U^{\dagger}(t,t_0)]$, which exists on the upper [lower] contour branch. It is often assumed, that a quantum system, which is driven out of equilibrium, starts out in a mixed state in thermal equilibrium, described by $H^M(t_0) = H(t_0) - \mu N(t_0)$, with the time t_0 at which the system starts propagating in time, the chemical potential μ and the particle number operator N. The mixed state with the inverse temperature β can be represented by the dessity operator

$$\rho = \frac{\exp^{-\beta H^M(t_0)}}{Z},$$

where $Z = tr\left(\exp^{-\beta H^M(t_0)}\right)$ is the thermal equilibrium partition function. Then the exponential can be viewed as a propagation in imaginary time up to $-i\beta$ along the Matsubara contour.

Usually an expectation value $\langle \cdots \rangle$ is obtained by splitting H_{imp} into a sum $H_{imp} = H_0 + H_{int}$, the time propagation is computed exactly in H_0 and H_{int} is treated by a formal pertubative expansion. For a weak electronic coupling, known as the weak-coupling approach, the expansion is performed in terms of the paramter U. In the strong-coupling approach, the one used in this thesis, a large U is assumed and H_D and H_B sum up to H_0 , while the expansion is performed in terms of H_{hyb}, which is demonstrated in the following.

In the interaction picture the operators, here denoted by a hat$\widehat{\ }$, have the time dependency

$$\hat{O}(t) = \exp^{iH_0t}\,\mathrm{O}\exp^{-iH_0t},$$

with the reduced Hamiltonian$H_0 = H_{imp} - H_{hyb}$ containing information about the electron coupling U. The interaction picture time evolution propagator is given by

$$U(t) = \exp^{iH_0t}\exp^{-iHt}$$

and obays the the differential equation

$$\frac{\partial}{\partial t}U(t) = i\exp^{iH_0t}(H_0 - H)\exp^{-iH_0t}$$
$$= -i\exp^{iH_0t}H_{hyb}(\exp^{-iH_0t}\exp^{iH_0t})\exp^{iHt}$$

$$= -i\widehat{H}_{hyb}(t)U(t).$$

After integrating both sides with respect to time

$$U(t) = 1 - i \int_0^t dt_1 \widehat{H}_{hyb}(t_1) U(t_1)$$

and after repeatedly iterating we arrive at

$$U(t) = \sum_{n=0}^{\infty} (-i)^n \int_0^t dt_1 \int_0^{t_1} dt_2 \cdots \int_0^{t_{n-1}} dt_n \widehat{H}_{hyb}(t_1) \widehat{H}_{hyb}(t_2) \cdots \widehat{H}_{hyb}(t_n) \tag{4}$$

with time ordering $t_1 > t_2 > \ldots > t_n$. The Hybridization term in the interaction picture can be written in the following form

$$\widehat{H}_{hyb}(t) = exp^{iH_0 t} V exp^{-iH_0 t}$$

$$= \sum_{n=0}^{\infty} \frac{i}{n!}^n (H_0 t)^n \sum_{\sigma,k} (v_{\sigma k} b_\sigma^\dagger d_\sigma + v_{\sigma k}^\star d_\sigma^\dagger b_\lambda) \sum_{\mathrm{n=0}}^{\infty} \frac{(-\mathrm{i})}{\mathrm{n!}}^{\mathrm{n}} (\mathrm{H_0 t})^{\mathrm{n}}$$

$$= \sum_{\sigma,k} \sum_{n=0}^{\infty} \frac{i}{n!}^n (\varepsilon_\sigma d_\sigma^\dagger d_\sigma + U n_\uparrow n_\downarrow + \varepsilon_k b_k^\dagger b_k)^n (t)^n \sum_{\sigma,k} (v_{\sigma k} b_\sigma^\dagger d_\sigma + v_{\sigma k}^\star d_\sigma^\dagger b_k) \sum_{\mathrm{n=0}}^{\infty} \frac{(-\mathrm{i})}{\mathrm{n!}}^{\mathrm{n}} (\varepsilon_\sigma \mathrm{d}_\sigma^\dagger \mathrm{d}_\sigma + \mathrm{U n}_\uparrow \mathrm{n}_\downarrow + \varepsilon_\lambda \mathrm{b}_\lambda^\dagger \mathrm{b}_\lambda)^{\mathrm{n}} (\mathrm{t})^{\mathrm{n}}$$

Using $[\mathrm{d}_\sigma, \mathrm{n}_\uparrow \mathrm{n}_\downarrow] = \mathrm{d}_{\bar{\sigma}}$ and Baker-Hausdorff theorem

$$d_\sigma(t) = exp^{iH_0 t} d_\sigma exp^{-iH_0 t} = exp^{-itL_{H_0}} d_\sigma,$$

where $L_{H_0} d_\sigma \equiv [d_\sigma, H_0] = \sum_{\sigma\epsilon\uparrow,\downarrow} \varepsilon_\sigma \left[d_\sigma, d_\sigma^\dagger d_\sigma\right] = \sum_{\sigma\epsilon\uparrow,\downarrow} \varepsilon_\sigma d_\sigma$, we arrive at

$$\widehat{H}_{hyb}(t) = \sum_{\sigma,k} \left\{ v_{\sigma k} exp^{i(\varepsilon_\sigma + U d_\sigma^\dagger d_\sigma - \varepsilon_{\sigma k})t} b_{\sigma k}^\dagger d_\sigma + v_{\sigma k}^\star exp^{-i(\varepsilon_\sigma + U d_\sigma^\dagger d_\sigma - \varepsilon_{\sigma k})t} d_\sigma^\dagger b_{\sigma k} \right\}.$$

- TODO: add contour

2.4.2 Green's function computation within the non-crossing approximation

Bold propagators

The first step is to compute so called bold propagators $G_{\alpha\beta}(t)$ between many the body states α and β containing all hybridization lines in a given time intervall that do not cross each other (therefore the name non-crossing approximation) and exist on one branch only. Propagators on the upper and lower branch obey the relation $G_{\alpha\beta}^\dagger(t) = G_{\alpha\beta}(\bar{t})$. Starting from the formal expression

$$G_{\alpha\beta}(t) = \langle\langle \alpha \mid \rho_D exp^{-iHt} \mid \beta \rangle\rangle_B = \langle\langle \alpha \mid \rho_D \exp^{-iH_0 t} U(t) \mid \beta \rangle\rangle_B,$$

where $\langle \cdots \rangle_B = Tr\left\{\rho_B \cdots\right\}$ denotes that the bath degrees are traced out, the expansion for the time evolution operator $U(t)$ 4 can be inserted

$$G_{\alpha\alpha}(t) = \langle\langle \alpha \mid \rho_D \exp^{-iH_0 t} \mid \alpha \rangle\rangle_B + (-i)^2 \int_0^t dt_1 \int_0^{t_1} dt_2 \langle\langle \alpha \mid \rho_D \exp^{-iH_0 t} \widehat{H}_{hyb}(t_1) \widehat{H}_{hyb}(t_2) \mid \alpha \rangle\rangle_B + \cdots$$

$$= \sum_{\beta} \langle\langle \alpha \mid \beta\rangle\langle\beta \mid \exp^{-iH_0 t} \mid \alpha\rangle\rangle_B - \sum_{\beta}\sum_{\sigma,\lambda} \int dt_1 \int_0^{t_1} dt_2 \, |t_{\sigma\lambda}|^2 \times$$

$$\Big(\langle\langle \alpha \mid \exp^{-iH_0 t} \, d_\sigma \mid \beta\rangle\langle\beta \mid d_\sigma^\dagger \hat{b}_{\sigma\lambda}^\dagger(t_1) \hat{b}_{\sigma\lambda}(t_2) \mid \alpha\rangle\rangle_B + \langle\langle \alpha \mid \exp^{-iH_0 t} \, d_\sigma^\dagger \mid \beta\rangle\langle\beta \mid d_\sigma \hat{b}_{\sigma\lambda}(t_2) \hat{b}_{\sigma\lambda}^\dagger(t_1) \mid \alpha\rangle\rangle_B \Big) + \cdots$$

$$= \delta_{\alpha\beta} \mathrm{exp}^{-\mathrm{i}\varepsilon_\alpha \mathrm{t}} - \sum_{\beta} \int_0^{\mathrm{t}} \mathrm{dt}_1 \int_0^{\mathrm{t}_1} \mathrm{dt}_2 \mathrm{G}_{\alpha\alpha}^{(0)}(\mathrm{t} - \mathrm{t}_1) \mathrm{G}_{\beta\beta}^{(0)}(\mathrm{t}_1 - \mathrm{t}_2) \times$$

$$\left(\langle \alpha \mid d_\sigma \mid \beta\rangle\langle\beta \mid d_\sigma^\dagger \mid \alpha\rangle \sum_{\sigma,\lambda} |t_{\sigma\lambda}|^2 \, \langle \hat{b}_{\sigma\lambda}^\dagger(t_1) \hat{b}_{\sigma\lambda}(t_2)\rangle_B + \langle \alpha \mid d_\sigma^\dagger \mid \beta\rangle\langle\beta \mid d_\sigma \mid \alpha\rangle \sum_{\sigma,\lambda} |t_{\sigma\lambda}|^2 \, \langle \hat{b}_{\sigma\lambda}(t_2) \hat{b}_{\sigma\lambda}^\dagger(t_1)\rangle_B \right) G_{\alpha\alpha}(t_2) + \cdots$$

$$= G_{\alpha\alpha}^{(0)}(t) - \sum_{\beta} \int_0^t dt_1 \int_0^{t_1} dt_2 G_{\alpha\alpha}^{(0)}(t - t_1) G_{\beta\beta}^{(0)}(t_1 - t_2) \times$$

$$\left(\langle \alpha \mid d_\sigma \mid \beta\rangle\langle\beta \mid d_\sigma^\dagger \mid \alpha\rangle \, \triangle_\sigma^< (t_1 - t_2) + \langle \alpha \mid d_\sigma^\dagger \mid \beta\rangle\langle\beta \mid d_\sigma \mid \alpha\rangle \, \triangle_\sigma^> (t_1 - t_2) \right) G_{\alpha\alpha}^{(0)}(t_2) + \cdots$$

with the bare atomic state propagators $G_{\alpha\alpha}^{(0)}(t) = \exp^{-i\varepsilon_\alpha t}$ leaving the dot state invariant. Both the bare $G_{\alpha\alpha}^{(0)}(t)$ and bold propagator $G_{\alpha\alpha}(t)$ are diagonal for the Anderson impurity model because the trace over the bath differs from zero only for an even number of creation and annhilation operators, therefore only square terms of $\widehat{H}_{hyb}$ appear in the expansion for the propagators. In DMFT the hybridization function $\Delta_\sigma^{>/<}$ is obtained from the self-consistency condition, but for the initial guess it can be expressed in terms of the coupling density $\Gamma(\omega) = \pi \sum_k \mid t_k \mid^2 \delta(\omega - \varepsilon_k)$ that fully describes the bath properties and the hybridization with the initial Fermi Dirac distribution $f(\omega - \mu) = \frac{1}{1+\exp^{\beta(\omega-\mu)}}$

$$\Delta^<(t_1, t_2) = \int_{-\infty}^{\infty} \frac{d\omega}{\pi} exp^{-i\omega(t_1 - t_2)} \Gamma(\omega) f(\omega - \mu) \tag{5}$$

and

$$\Delta^>(t_1, t_2) = \int_{-\infty}^{\infty} \frac{d\omega}{\pi} exp^{-i\omega(t_1 - t_2)} \Gamma(\omega)(1 - f(\omega - \mu)).$$

With the approximation for the self-energy, that it includes only non-crossing hybridizaton lines, the Dyson equation can be written as

$$G_{\alpha\alpha}(t) = G_{\alpha\alpha}^{(0)}(t) - \int_0^t dt_1 \int_0^{t_1} dt_2 G_{\alpha\alpha}^{(0)}(t - t_1) \Sigma_{\alpha\alpha}(t_1 - t_2) G_{\alpha\alpha}(t_2)$$

with

$$\Sigma_{\alpha\alpha}(t_1 - t_2) = \sum_{\sigma}\sum_{\beta} G_{\beta\beta}(t_1 - t_2) \times$$

$$\left(\langle \alpha \mid d_\sigma \mid \beta\rangle\langle\beta \mid d_\sigma^\dagger \mid \alpha\rangle \Delta_\sigma^<(t_1 - t_2) + \langle \alpha \mid d_\sigma^\dagger \mid \beta\rangle\langle\beta \mid d_\sigma \mid \alpha\rangle \Delta_\sigma^>(t_1 - t_2) \right).$$

For the four different initial states, denoted by the outer index α, on the dot a set of coupled Dyson equations is derived

$$G_0(t) = G_0^{(0)}(t) - \int_0^t dt_1 \int_0^{t_1} dt_2 G_0^{(0)}(t-t_1) G_\uparrow(t_1-t_2)\Delta_\uparrow^<(t_1-t_2) G_0(t_2) - \int_0^t \mathrm{dt}_1 \int_0^{t_1} \mathrm{dt}_2 \mathrm{G}_0^{(0)}(\mathrm{t}-\mathrm{t}_1)\mathrm{G}_\downarrow(\mathrm{t}_1-\mathrm{t}_2)\Delta_\downarrow^<(\mathrm{t}_1-\mathrm{t}_2)\mathrm{G}_0(\mathrm{t}_2)$$

$$G_\uparrow(t) = G_\uparrow^{(0)}(t) - \int_0^t dt_1 \int_0^{t_1} dt_2 G_\uparrow^{(0)}(t-t_1) G_0(t_1-t_2)\Delta_\uparrow^>(t_1-t_2) G_\uparrow(t_2) - \int_0^t \mathrm{dt}_1 \int_0^{t_1} \mathrm{dt}_2 \mathrm{G}_\uparrow^{(0)}(\mathrm{t}-\mathrm{t}_1)\mathrm{G}_{\uparrow\downarrow}(\mathrm{t}_1-\mathrm{t}_2)\Delta_\downarrow^<(\mathrm{t}_1-\mathrm{t}_2)\mathrm{G}_\uparrow(\mathrm{t}_2)$$

$$G_\downarrow(t) = G_\downarrow^{(0)}(t) - \int_0^t dt_1 \int_0^{t_1} dt_2 G_\downarrow^{(0)}(t-t_1) G_0(t_1-t_2)\Delta_\uparrow^>(t_1-t_2) G_\downarrow(t_2) - \int_0^t \mathrm{dt}_1 \int_0^{t_1} \mathrm{dt}_2 \mathrm{G}_\downarrow^{(0)}(\mathrm{t}-\mathrm{t}_1)\mathrm{G}_{\uparrow\downarrow}(\mathrm{t}_1-\mathrm{t}_2)\Delta_\downarrow^<(\mathrm{t}_1-\mathrm{t}_2)\mathrm{G}_\downarrow(\mathrm{t}_2)$$

$$G_{\uparrow\downarrow}(t) = G_{\uparrow\downarrow}^{(0)}(t) - \int_0^t dt_1 \int_0^{t_1} dt_2 G_{\uparrow\downarrow}^{(0)}(t-t_1) G_\downarrow(t_1-t_2)\Delta_\uparrow^>(t_1-t_2) G_{\uparrow\downarrow}(t_2) - \int_0^t \mathrm{dt}_1 \int_0^{t_1} \mathrm{dt}_2 \mathrm{G}_{\uparrow\downarrow}^{(0)}(\mathrm{t}-\mathrm{t}_1)\mathrm{G}_\uparrow(\mathrm{t}_1-\mathrm{t}_2)\Delta_\downarrow^>(\mathrm{t}_1-\mathrm{t}_2)\mathrm{G}_{\uparrow\downarrow}(\mathrm{t}_2),$$

which can be solved by a self consistent iteration. In equilibirum all entities depend only on time differences and one can evaluate the integrals in the Fourier space, where convolutions correspond to multiplications. Solving these above equations for non-equilibirum system is more complex and will be treated in the next chapter. Before starting with the first iteration, the bold propagators $\mathrm{G}_{\alpha\alpha}(\mathrm{t})$ are initialized by the bare propagators $\mathrm{G}_{\alpha\alpha}^{(0)}(\mathrm{t})$ from which the first self-energy is obtained. Both are inserted into the Dyson equation with the interaction times integrated over. With the updated $\mathrm{G}_{\alpha\alpha}(\mathrm{t})$ one can go back to the second step and compute a new self energy for the next iteration cycle until convergence is reached.

Correlation functions

So far we have calculated propagators between many body states, which contain all non-crossing hybridization lines in a time segment on a single branch. These objects have no physical meaning and in torder to compute physical observables it is necessary to include hybridization lines connecting times on both branches. We introduce so called vertex functions $\mathrm{K}_{\alpha\beta}(\mathrm{t},\mathrm{t}')$ with the first[second] time index on the upper[lower] branch. A vertex funcion incorporates all non-crossing intra- and inter-branch hybrdization lines. The procedure to estimate $\mathrm{K}_{\alpha\beta}(\mathrm{t},\mathrm{t}')$ is similar to the calculation of $\mathrm{G}_{\alpha\alpha}(\mathrm{t})$ with the difference that $\mathrm{K}_{\alpha\beta}(\mathrm{t},\mathrm{t}')$ is a two-times function and instead of four we have 16 equations representing the evolution of the dot from any inital state α to any final state β. For every inital state there are four coupled equations of the form

$$K_{\alpha\beta}(t,t') = K_{\alpha\beta}^{(0)}(t,t') + \sum_{\gamma\delta} \int_0^t dt_1 \int_0^{t'} dt_2 K_{\alpha\gamma}(t_1,t_2)\mathbf{\Delta}_{\gamma\delta}(t_1,t_2) G_{\delta\beta}^\dagger(t-t_1) G_{\delta\beta}(t'-t_2).$$

The vertex functions without inter-branch hybridization lines are composed by the bold propagators on the upper and lower branch

$$K^{(0)}_{\alpha\beta}(t,t') = \delta_{\alpha\beta} G^{\dagger}_{\alpha\beta}(t) G_{\alpha\beta}(t').$$

The self consistent equations for the initially unoccupied dot are

$$K_{00}(t,t') = K^{(0)}_{00}(t,t') + \int_0^t dt_1 \int_0^{t'} dt_2 G^{\dagger}_0(t'-t_2) G_0(t-t_1) \Delta^{<}_{\uparrow}(t_1,t_2) K_{0\uparrow}(t_1,t_2) + \int_0^{\mathrm{t}} \mathrm{dt}_1 \int_0^{\mathrm{t}'} \mathrm{dt}_2 \mathrm{G}^{\dagger}_0(\mathrm{t}'-\mathrm{t}_2) \mathrm{G}_0(\mathrm{t}-\mathrm{t}_1) \Delta^{<}_{\downarrow}(\mathrm{t}_1,\mathrm{t}_2) \mathrm{K}_{0\downarrow}(\mathrm{t}_1,\mathrm{t}_2)$$

$$K_{0\uparrow}(t,t') = \int_0^t dt_1 \int_0^{t'} dt_2 G^{\dagger}_{\uparrow}(t'-t_2) G_{\uparrow}(t-t_1) \Delta^{>}_{\uparrow}(t_1,t_2) K_{00}(t_1,t_2) + \int_0^{\mathrm{t}} \mathrm{dt}_1 \int_0^{\mathrm{t}'} \mathrm{dt}_2 \mathrm{G}^{\dagger}_{\uparrow}(\mathrm{t}'-\mathrm{t}_2) \mathrm{G}_{\uparrow}(\mathrm{t}-\mathrm{t}_1) \Delta^{<}_{\downarrow}(\mathrm{t}_1,\mathrm{t}_2) \mathrm{K}_{0\uparrow\downarrow}(\mathrm{t}_1,\mathrm{t}_2)$$

$$K_{0\downarrow}(t,t') = \int_0^t dt_1 \int_0^{t'} dt_2 G^{\dagger}_{\downarrow}(t'-t_2) G_{\downarrow}(t-t_1) \Delta^{>}_{\downarrow}(t_1,t_2) K_{00}(t_1,t_2) + \int_0^{\mathrm{t}} \mathrm{dt}_1 \int_0^{\mathrm{t}'} \mathrm{dt}_2 \mathrm{G}^{\dagger}_{\downarrow}(\mathrm{t}'-\mathrm{t}_2) \mathrm{G}_{\downarrow}(\mathrm{t}-\mathrm{t}_1) \Delta^{<}_{\uparrow}(\mathrm{t}_1,\mathrm{t}_2) \mathrm{K}_{0\uparrow\downarrow}(\mathrm{t}_1,\mathrm{t}_2)$$

$$K_{0\uparrow\downarrow}(t,t') = \int_0^t dt_1 \int_0^{t'} dt_2 G^{\dagger}_{\uparrow\downarrow}(t'-t_2) G_{\uparrow\downarrow}(t-t_1) \Delta^{>}_{\downarrow}(t_1,t_2) K_{0\uparrow}(t_1,t_2) + \int_0^{\mathrm{t}} \mathrm{dt}_1 \int_0^{\mathrm{t}'} \mathrm{dt}_2 \mathrm{G}^{\dagger}_{\uparrow\downarrow}(\mathrm{t}'-\mathrm{t}_2) \mathrm{G}_{\uparrow\downarrow}(\mathrm{t}-\mathrm{t}_1) \Delta^{>}_{\uparrow}(\mathrm{t}_1,\mathrm{t}_2) \mathrm{K}_{0\downarrow}(\mathrm{t}_1,\mathrm{t}_2).$$

For equal times, $K_{\alpha\beta}(t,t)$ is the population probability on the dot. After initializing the vertex functions $K_{\alpha\beta}(t,t')$ with $K^{(0)}_{\alpha\beta}(t,t')$ and performing the self-consistent iteration sheme one is able to construct Greens functions in the following way

$$G^{>}_{\alpha\uparrow}(t,t') = -i\langle \mathrm{d}_{\uparrow}(\mathrm{t}) \mathrm{d}^{\dagger}_{\uparrow}(\mathrm{t}') \rangle = K_{\alpha 0}(t,t') * G_{\uparrow}(t-t') + K_{\alpha\downarrow}(t,t') * G_{\uparrow\downarrow}(t-t')$$

$$G^{<}_{\alpha\uparrow}(t,t') = i\langle \mathrm{d}^{\dagger}_{\uparrow}(\mathrm{t}') \mathrm{d}_{\uparrow}(\mathrm{t}) \rangle = K_{\alpha\uparrow}(t,t') * G_0(t-t') + K_{\alpha\uparrow\downarrow}(t,t') * G_{\downarrow}(t-t')$$

$$G^{>}_{\alpha\downarrow}(t,t') = -i\langle \mathrm{d}_{\downarrow}(\mathrm{t}) \mathrm{d}^{\dagger}_{\downarrow}(\mathrm{t}') \rangle = K_{\alpha 0}(t,t') * G_{\downarrow}(t-t') + K_{\alpha\uparrow}(t,t') * G_{\uparrow\downarrow}(t-t')$$

$$G^{<}_{\alpha\downarrow}(t,t') = i\langle \mathrm{d}^{\dagger}_{\downarrow}(\mathrm{t}') \mathrm{d}_{\downarrow}(\mathrm{t}) \rangle = K_{\alpha\downarrow}(t,t') * G_0(t-t') + K_{\alpha\uparrow\downarrow}(t,t') * G_{\uparrow}(t-t')$$

with α denoting the initial dot state.

- TODO: Add schematic representation of diagrams.

2.4.3 Properties of the Green's functions

The retarded and advanced component of the Green's function are linked via

$$G^R(t,t') = \left[G^A(t',t)\right]^*$$

and can be defined via the lesser and greater component as

$$G^R(t,t') = -i\Theta(t-t')\langle\left[d(t), d^\dagger(t')\right]_+\rangle$$

$$G^R(t,t') = -i\Theta(t-t')\left(\langle d(t)d^\dagger(t')\rangle + \langle d^\dagger(t')d(t)\rangle\right)$$

$$G^R(t,t') = \Theta(t-t')\left(G^>(t,t') - G^<(t,t')\right)$$

and

$$G^A(t,t') = i\Theta(t'-t)\langle\left[d(t), d^\dagger(t')\right]_+\rangle$$

$$G^A(t,t') = i\Theta(t'-t)\left(\langle d(t)d^\dagger(t')\rangle + \langle d^\dagger(t')d(t)\rangle\right)$$

$$G^A(t,t') = -\Theta(t'-t)\left(G^>(t,t') - G^<(t,t')\right).$$

The lesser and greater component fulfil

$$-G^{>/<}(t,t') = \left[G^{>/<}(t,t')\right]$$

and for particle-hole symmetric system they hold

$$G^{>/<}(t,t') = -G^{>/<}(t',t).$$

The imaginary part of their Fourier transforms gives an intuitive interpretation in terms of the spectral function $A(\omega)$, which corresponds to the density of states.

$$A(\omega) = -\frac{1}{\pi} ImG(\omega)^R = \frac{1}{\pi} ImG(\omega)^A.$$

Out of equilibrium one can still define a spectral function via a partial Fourier transform

$$A(\omega, t_{av}) = -\frac{1}{\pi} Im \int dt_{rel} \exp^{i\omega t_{rel}} G^R(t,t'),$$

with $t_{av} = (t+t')/2$ and $t_{rel} = t - t'$ and which satisfies

$$\int d\omega A(\omega) = 1.$$

The lesser [greater] Green's function contains information about the distribution of occupied [unoccupied] states

$$\mp ImG^<(\omega) = 2\pi A(\omega) n(\omega)$$

$$-ImG^>(\omega) = 2\pi A(\omega)[1 \pm n(\omega)].$$

The upper signs are valid for bosons and the lower for fermions. Here, $n(\omega)$ represents the nonequilibrium distribution function, in equilibrium coincides with the Bose or Fermi distribution.

2.5 Time-dependent electric fields

Within non-equilibrium DMFT many physical problems, like the application of electromagnetic driving fields, can be treated. A time-dependent electromagnetic field converts the hopping term $v_{ij}(t)$ into

$$v_{ij}(t) = v_{ij} \exp\left(-\frac{ie}{\hbar}\int_{\vec{R}_i}^{\vec{R}_j} d\vec{r}\vec{A}(\vec{r},t)\right),$$

where the vector potential $\vec{A}(\vec{r},t)$ is treated as a phase factor and a scalar potential term $e\sum_{i\sigma}\Phi(\vec{R}_i,t)d^\dagger_{i\sigma}d_{i\sigma}$ is added to the Hamiltonian. This corresponds to a Pierls substitution, which is derived from the requirement that the Hamiltonian is gauge-invariant. With a time-dependent hopping the self-consistency condition for a semi-circular density of states generalizes from to

$$\Delta(t,t') = v(t)G(t,t')v^*(t').$$

Applying an unpolarized AC electric field propagating in the z-direction results in a time-periodic linear potential originating from the root of the Bethe lattice via a driving term

$$H_{drv}(t) = \sum_j eaE_0 sin(\omega t)s_j n_j,$$

with the electric charge e, the amplitude of the field E_0, the angular frequency of the driving ω and s_j the number of steps from the root of the tree to site j. Performing the unitary transformation

$$U(t) = \exp\left[i\phi(t)\sum_j s_j n_j\right],$$

where $\phi(t) = -(eaE_0/\omega)cos(\omega t)$, the full Hamiltonian $H(t) = H_{Hub} + H_{drv}(t)$ can be transformed into the rotating-frame Hamiltonian

$$H_{rot}(t) = i\frac{dU(t)}{dt}U^\dagger(t) + U(t)H(t)U^\dagger(t)$$

$$= -i\sum_l eaE_0 sin(\omega t)s_l n_l \exp\left[i\phi(t)\sum_l s_l n_l\right]\exp\left[-i\phi(t)\sum_k s_k n_k\right] +$$

$$\exp\left[i\phi(t)\sum_l s_l n_l\right]\left[-\sum_{\langle i,j\rangle,\sigma} v_{ij}d^\dagger_{i\sigma}d_{j\sigma} + \sum_i U(d^\dagger_{i\uparrow}d_{i\uparrow} - \frac{1}{2})(d^\dagger_{i\downarrow}d_{i\downarrow} - \frac{1}{2}) + \sum_i eaE_0 sin(\omega t)s_i n_i\right]\exp\left[-i\phi(t)\sum_k s_k n_k\right]$$

$$= -\sum_l eaE_0 sin(\omega t)s_l n_l \exp\left[\phi(t)\sum_l s_l n_l\right]\exp\left[i\phi(t)\sum_k s_k n_k\right] +$$

$$\exp\left[i\phi(t)\sum_l s_l n_l\right] i\sum_l eaE_0 sin(\omega t)s_l n_l \exp\left[i\phi(t)\sum_k s_k n_k\right] +$$

$$(1+i\phi(t)\sum_l s_l n_l+...)\times-\sum_{\langle i,j\rangle,\sigma} v_{ij}d^\dagger_{i\sigma}d_{j\sigma}\times-(1+i\phi(t)\sum_k s_k n_k+...)+$$

$$(1+i\phi(t)\sum_l s_l n_l+...)\times-\sum_i U(d^\dagger_{i\uparrow}d_{i\uparrow}-\frac{1}{2})(d^\dagger_{i\downarrow}d_{i\downarrow}-\frac{1}{2})\times-(1+i\phi(t)\sum_k s_k n_k+...)+$$

$$=eaE_0 sin(\omega t)s_k\times\exp\left[\phi(t)\sum_l s_l n_l\right]\exp\left[i\phi(t)\sum_k s_k n_k\right]\times\sum_{l\neq k} eaE_0 sin(\omega t)s_l n_l\times(1-1)+$$

$$\exp\left[-i\phi(t)s_k\right]\exp\left[i\phi(t)s_l\right]\times-\sum_{\langle i,j\rangle,\sigma} v_{ij}d^\dagger_{i\sigma}d_{j\sigma}\times\exp\left[i\phi(t)\sum_{k\neq i,j} s_k n_k\right]\exp\left[-i\phi(t)\sum_{l\neq i,j} s_l n_l\right]+$$

$$\exp\left[-i\phi(t)s_i\right]\exp\left[i\phi(t)s_i\right]\times-\sum_i U(d^\dagger_{i\uparrow}d_{i\uparrow}-\frac{1}{2})(d^\dagger_{i\downarrow}d_{i\downarrow}-\frac{1}{2})\times\exp\left[i\phi(t)\sum_{k\neq i} s_k n_k\right]\exp\left[-i\phi(t)\sum_{l\neq i} s_l n_l\right]$$

This results in the elimination of the driving term. The rotating frame Hamiltonian H_{rot} and H_{Hub} differ only by a time-dependent Pierls phase on the hopping amplitude

$$v_{ij}(t)=v_{ij}\exp^{iA(s_i-s_j)cos(\omega t)}.$$

The factor $(s_i-s_j)=\pm1$ implies nearest neighbor hopping and we define the dimensionless driving amplitude as $A=eaE_0/\omega$.

2.6 Dissipative systems

Real materials can exchange energy and particles with their environment, which should be included into the description of our system. Continuously driving an open system with an external field enables the energy injected into the system to dissipate into the bath and the emergence of a steady state.

One can describe dissipation of energy to other degrees of freedom by coupling every site of the lattice to an environment. In DMFT two dissipation mechanisms have been adopted so far. The first one couples each lattice site to a reservoir of non-interacting fermions. The free-fermion bath has the same structure as the bath in the Anderson impurity model and is defined by

$$H_f=H_{fBath}+H_{fmix} \tag{6}$$

$$H_{fBath}=\sum_{k,\sigma}\varepsilon_k f^\dagger_{k,\sigma}f_{k,\sigma}$$

and

$$H_{fmix}=\sum_{k,\sigma}(V_k f^\dagger_{k,\sigma}d_\sigma+V^*_k d^\dagger_\sigma f_{k,\sigma}),$$

where $d_\sigma^\dagger(d_\sigma)$ creates (annihilates) an electron on the dot, $f_k^\dagger(f_k)$ creates (annihilates) a bath degree of freedom, ε_k describes the bath energy levels and V_k is the hybridization between the bath modes and the impurity. The bath is in thermal equilibrium with a defined tamperature T and a chemical potential μ_k, which is chosen such that there is no current flow between the bath and the impurity. Since the bath has a bilinear structure it can be integrated out analytically and it turns out that it contributes to the system through an additional self-energy correction. The Dyson equation can be symbolically written as

$$G(t,t') = (G_0^{-1}(t,t') - \Sigma_{fBath}(t,t') - \Sigma(t,t'))^{-1}, \tag{7}$$

where all objects are matrices and the bath self-energy is given by

$$\Sigma_{fBath}^{\alpha\alpha}(t,t') = \sum_\beta G^{\beta\beta}(t,t') \times \Lambda_\beta^{\alpha\alpha}(t,t')$$

with the bath hybridization function $\Lambda_\beta^{\alpha\alpha}(t,t')$ defined via the coupling densities $\Gamma(\omega) = \pi \sum_k V_k V_k^* \delta(\omega + \mu_k - \epsilon_{k,\sigma})$ and the initial occupation given by the Fermi-Dirac distribution like in 5.

The second dissipation mechanism is the coupling to a bosonic bath, which can be described via the Holstein coupling with the local phonon bath Hamiltonian

$$H_{phBath} = \sum_q \omega_q b_q^\dagger b_q.$$

Here $b_q^\dagger(b_q)$ are creation (annihilation) operators and ω_q is the frequency of the phonon mode q. The electron-phonon coupling is given by

$$H_{phMix} = \sum_q \lambda_q (b_q^\dagger + b_q)(n_d - 1),$$

where n_d is the total dot occupation and λ_d the coupling strength between the dot and the phonon modes. The factor -1 has no physical meaning, but is there to sustain particle-hole symmetry for the energy level $\epsilon = 0$. The properties of the bath are fully defined by the spectral function $J(\omega) = \pi \sum_q \frac{\lambda_q^2}{\omega_q} \delta(\omega - \omega_q)$. We assume that the coupling to the phonon bath is weak and perform second order pertubation theory. Similar to 7 the Dyson equation takes the form

$$G(t,t') = (G_0^{-1}(t,t') - \Sigma_{phBath}(t,t') - \Sigma(t,t'))^{-1},$$

but here the phonon self-energies do not change the state of the dot:

$$\Sigma_{phBath}^{\alpha\alpha}(t,t') = G^{\alpha\alpha}(t,t') \times \Lambda^{\alpha\alpha}(t,t').$$

The phonon Hybridization function is defined by

$$\Lambda^{\alpha\alpha}(t,t') = <\alpha|(n_d(t)-1)(n_d(t')-1)|\alpha> \times \sum_q \lambda_q^2 Tr_b[\rho_b((b_q^\dagger(t) + b_q(t'))(b_q^\dagger(t) + b_q(t'))]$$

and if we consider that the bath is composed of free harmonic phonon modes we can write it as $\Lambda^{\alpha\alpha}(t-t') = (n_d^{(\alpha)} - \delta)^2 \times \Lambda_b(t-t')$, where

$$\Lambda_b(t-t') = \sum_q \lambda_q^2 B_q(t-t').$$

As for the fermion bath, the spectral function $J(\omega) = \frac{2}{\pi}\sum_q(\lambda_q^2/\omega_q)\delta(\omega-\omega_q)$ describes the properties of the phonon bath and $\Lambda_b(t-t')$ becomes

$$\Lambda_b(t-t') = \frac{2}{\pi}\int d\omega J(\omega)\omega B_\omega(t-t').$$

- TODO: Add schematic representation of an reservoir coupled to every lattice site.

3 Implementation

3.1 Bethe lattice

We will focus on the Hubbard model for a Bethe lattice in the limit of infinite dimensions, where DMFT becomes exact. With its semicircular Density of states

$$D(\epsilon) = \frac{1}{2\pi v_0^2}\sqrt{4v_0-\epsilon^2} \tag{8}$$

it relates the Greens function to the hybridization function in the simple way

$$\Delta(\omega) = v_0^2 G(\omega). \tag{9}$$

- TODO: graph of Bethe lattice structure and non-interacting DOS

3.2 Initial setup

The systems starts from in initial Néel state, which is a classical antiferromagnetic state

$$\mid \psi_{Neel} >= \prod_{i\epsilon A} d_{i\uparrow}^\dagger \prod_{j\epsilon B} d_{j\downarrow}^\dagger \mid 0 > .$$

It can be described by two identical sublattices with opposite magnetization, lattice A describing $\sigma =\uparrow$ and lattice B $\sigma =\downarrow$. It is sufficient to calculate the dynamics if only one sublattice since they obey the symmetry $G_{A,\sigma} = G_{B,-\sigma}$. The self-consistency condition for the Bethe lattice reads

$$\Delta_{A(B),\sigma}(t,t') = v(t)G_{B(A),\sigma}(t,t')v^*(t')$$

and using the symmetry it becomes

$$\Delta_\sigma(t,t') = v(t)G_{-\sigma}(t,t')v^*(t').$$

- Half filling
- Symmetries
- Two different lattice structures

3.3 Dissipation

The simplest treatment of the dissipation is to chose Γ to be a flat density of states with a soft cutoff $\Gamma(\omega) = \frac{\lambda}{(1+\exp^{\nu(\omega-\omega_c)})(1+\exp^{-\nu(\omega+\omega_c)})}$ ($\nu = \omega_c = 10$ and $\lambda = \Gamma(0)$).

3.4 Physical observables

The observable we are interested in measures the energy that flows between the system and the heat bath and can be obtained from $I_E(t) = \langle \mathcal{I}_E(t) \rangle$. The energy current $\mathcal{I}_E(t)$ is defined as

$$\mathcal{I}_E = \dot{H}_{fBath} = i[H, H_{fBath}] + \frac{\partial H_{fBath}}{\partial t},$$

with $H = H_D + H_B + H_{hyb} + H_{fBath} + H_{fMix}$ describing the original Anderson impurity Hamiltonian 3. This leads to

$$\mathcal{I}_E = i[\sum_{k,\sigma}(V_k f^\dagger_{k,\sigma} d_\sigma + V_k^* d^\dagger_\sigma f_{k,\sigma}), \sum_{k',\sigma'} \varepsilon_{k'} f^\dagger_{k',\sigma'} f_{k',\sigma'}]$$

$$= i\sum_{k,\sigma}(V_k f^\dagger_{k,\sigma} d_\sigma + V_k^* d^\dagger_\sigma f_{k,\sigma})\varepsilon_k f^\dagger_{k,\sigma} f_{k,\sigma} - i\sum_{k,\sigma} \varepsilon_k f^\dagger_{k,\sigma} f_{k,\sigma}(V_k f^\dagger_{k,\sigma} d_\sigma + V_k^* d^\dagger_\sigma f_{k,\sigma})$$

$$= i\sum_{k,\sigma} \varepsilon_k (V_k d_\sigma f^\dagger_{k,\sigma} - V_k^* f_{k,\sigma} d^\dagger_\sigma).$$

The energy current operator can be obtained by summing over all diagrams that have a special hybridization line that places the current operator at the tip of the Keldysh contour

$$I_E(t) = \int_0^t d\tau \Delta_f^<(t,\tau) G^<(t,\tau),$$

with the energy hybridization function $\Delta_f^<(t,\tau) = \int_{-\infty}^{\infty} \frac{d\omega}{\pi} exp^{-i\omega(t-\tau)} \omega \Gamma(\omega) f(\omega - \mu)$.

3.5 Numerical implementation

Working with non-equilibrium systems involves explicit time dependence, so that all objects become two times functions. In order to solve the impurity problem, we need to solve Dyson equations of the form

$$G_{\alpha\alpha}(t,t') = G^{(0)}_{\alpha\alpha}(t,t') - \int_0^t dt_1 \int_0^{t_1} dt_2 G^{(0)}_{\alpha\alpha}(t,t_1)\Sigma_{\alpha\alpha}(t_1,t_2)G_{\alpha\alpha}(t_2,t').$$

These are two-dimensional Volterra integral equations, which have a causal structure as the integral limits show. We compute every time-slice t by starting with $G_{\alpha\alpha}(t,t)$ and successively increasing t'.

TODO: Add graphic representation of how the matrix is filled out.

4 Results

4.1 Equilibrium properties

- TODO: show how non-interacting DOS splits to a Mott insulator at high U

4.2 Magnetic relaxation in a periodically driven Hubbard model

Before exploring new physics, we want to reproduce well known phenomena. In their recent research Martin Eckstein and al. studied the melting of long-range antiferromagnetic order in a periodically driven repulsive Hubbard model. This chapter is orientated on their paper and reproduces part of the results. We are calculating the dynamics with non-equilibrium DMFT for a Bethe-lattice in infinite dimensions. First we investigate the melting in the absence of a driving field and in a second step we explore the effect of a strong driving field in the case of a resonant driving frequency. The two quantities we are focusing on are the double occupation $d(t) =< n_\uparrow(t)n_\downarrow(t) >$, which is measuring the formation of charge excitations and the magnetization $M(t) = \frac{<n_\uparrow(t)-n_\downarrow(t)>}{1-2d(t)}$ as an indicator for the antiferromagnetic order of the the system. The magnetization $M(t)$ is formed by the straggered magnetic order parameter, which is normalizes by the probability of a site being sinlgy occupied.

4.2.1 Undriven magnetic melting

To begin with, we will look at the melting mechanisms in different regimes in the undriven case ($A = 0$, $v = v_0 = 1$). In the Mott-insulating regime with a strong Coulomb interaction $U \gg v$, Fig. ? shows the magnetic order parameter $M(t)$ and the double occupation $d(t)$ for different values of U during the timeslice $0 \leq v_0 t \lesssim 6$. The dynamics of both entities start with oscillations at short times resulting from the Néel state not being an eigenstate of the Hubbard model at finite U and change their behavior after $v_0 t \simeq 1$. The formation of charge excitations relaxes fastly to a U dependent steady state value at a low rate since the strong Coulomb interaction is preventing electrons to hop across the lattice and the magnetization $M(t)$ shows a linear decrease with a U dependent gradient. The fast relaxation of the charge dynamics compared to the magnetization indicates that the magnetic melting is due to the movement of the charge excitations on top of the anti-ferromagnetic spin background. To further underpin this statement Eckstein and al. investigated the spin precession dynamics by flipping an initially located fermion at a single probe site in the x direction. An effective magnetic field B_{eff}, which is formed by the neighbouring sites, is orientated along the z direction leading to harmonic precession of the magnetic moment in the x-y plane. It turns out that the precessing magnetic moment sustains, even for times $v_0 t > 1$, which confirms that the decay of the magnetic order is due to mobile charge excitations and local magnetic moments are preserved.

When the Coulomb interaction is lowered, coming close to the non-interacting limit $U = 0$, one expects quasiparticles to be responsible for the dynamics of the system. For $U \lesssim 1$ the magnetization shows an oscillatory behaviour and decays to zero fastly, while $d(t)$ relaxes to high values (Fig. ?). Compared to the results for $U \gg v$, where the spin dynamics relax much slower than the charge dynamics, here $M(t)$ and $d(t)$ both relax around $v_0 t \simeq 1$, indicating that the destruction of the anti ferromagnetic order is caused by the destruction of local magnetic moments.

Figure 2: Dynamics of our system without driving for high Coulomb interactions. Top: Decay of magnetic order parameter $M(t)$. Bottom: Decay of double occupation $d(t)$. Zoom into short time dynamics, because we refer to it in the text.

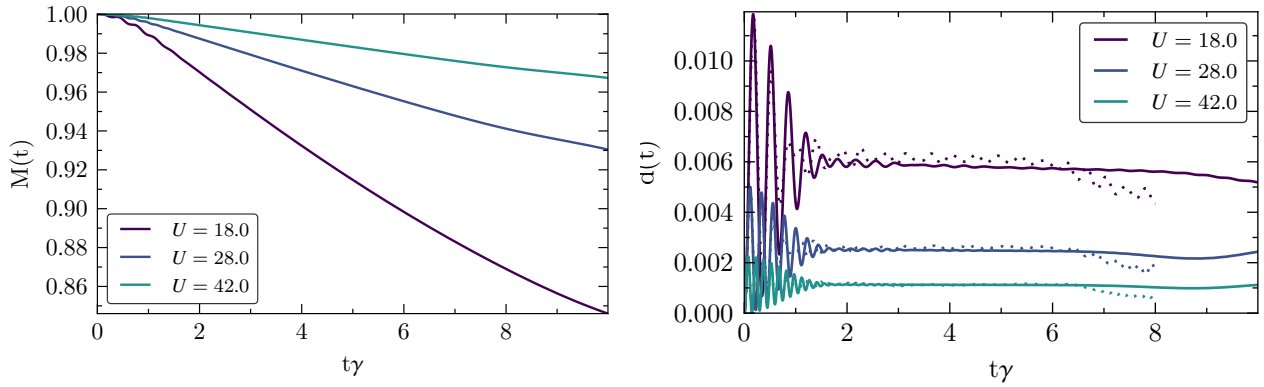

4.2.2 Magnetic melting in resonant driven lattices

Martin Eckstein and al are exploring the effects of an electric driving field in three different regimes: the high frequency, the resonant and in gap away from resonant driving regime. In this chapter we will focus only on the case of resonant driving, which modifies the behaviour of $M(t)$ and $d(t)$ strongly, changing the magnetization from a slow decay in the absence of driving to a fast decay even for small driving amplitudes. The double occupation goes from a saturation at low values to high values resembling the case for $U \lesssim 1$. Resonant driving is a tool to switch from the charge-excitation to the quasiparticle melting mechanism and control the relaxation speed of the charge and spin dynamics.

- TODO: explain attractive interaction

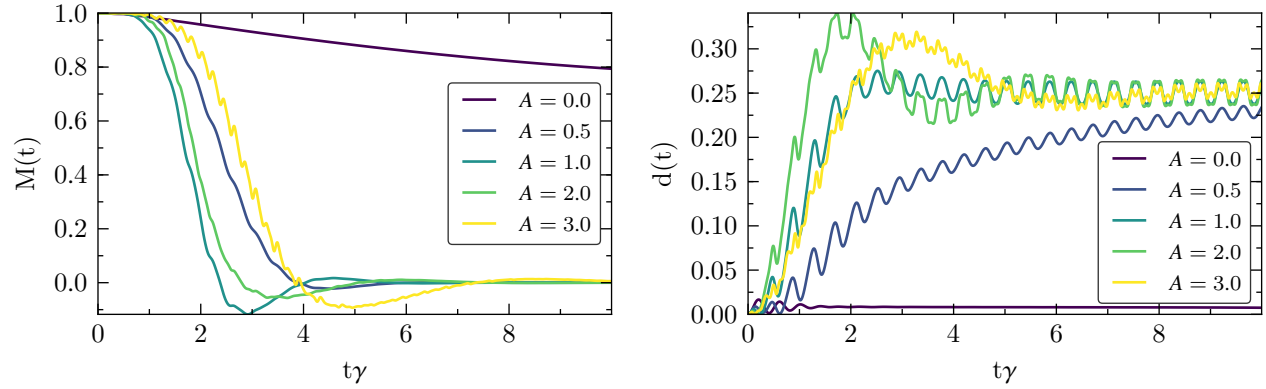

Figure 3: Dynamics of our system with $U = \omega = 15$ and various amplitudes. Left: Decay of magnetic order parameter $M(t)$. Right: Decay of double occupation $d(t)$.

4.3 Energy dissipation in a periodically driven system

We want to investigate how the system's response to a small pertubation changes when it is driven out of equilibrium. The response $P_{\omega_{probe}}(A_{probe})$ is defined as the energy current derivative with respect to the probe amplitude $A_{probe}(\omega_{probe})$

$$P_{\omega_{probe}}(A_{probe}) = \lim_{A_{probe}\to 0} \frac{dI_E(A_{probe}(\omega_{probe}))}{dA_{probe}(\omega_{probe})} \simeq \frac{I_E(\Delta A_{probe}(\omega_{probe}))}{\Delta A_{probe}(\omega_{probe})} = \frac{I_E(A_{probe}(\omega_{probe})) - I_E(A_{probe=0}(\omega_{probe}))}{A_{probe}(\omega_{probe}) - A_{probe=0}(\omega_{probe})}.$$

An example of the energy current4.3 at resonant driving shows that a steady state emerges after $v_0 t \simeq 3$. We are taking the average value of $P_{\omega_{probe}}$ over a period T to estimate the amout of energy that is flowing into the heat bath, which we will name $\bar{P}_{\omega_{probe}}$. The errorbars are calculated from the difference of $\overline{P}_{\omega_{probe}}$ between two periods.

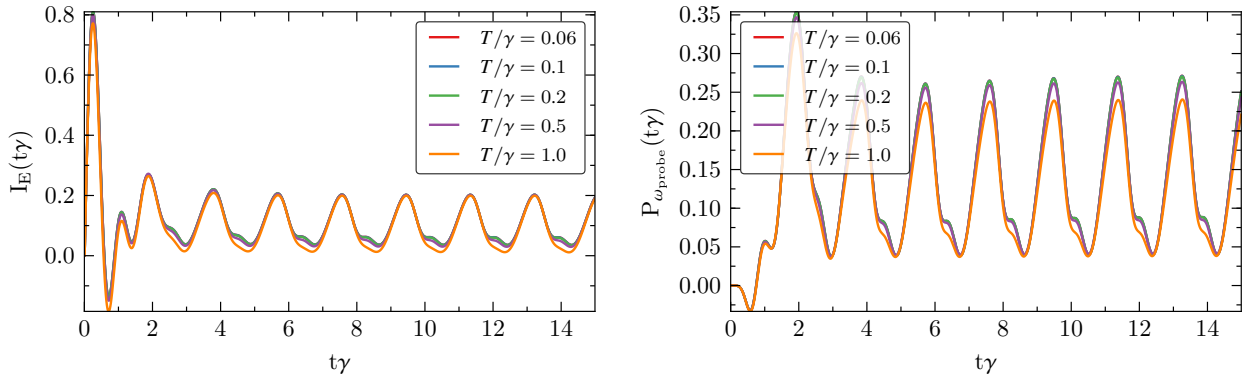

Figure 4: Left: Heat current for $A_{pump} = 1.0, \omega_{pump} = \omega_{probe} = 5$ and $A_{probe} = 0.1$. Right: Relative current for the same parameters

4.3.1 Unphysical Bethe lattice

Resonant driving at intermediate U

We start discussing results for a Coulomb interaction of $U = 5$ while the system is exposed to an electric field with the frequency of the bandgap and various amplitudes. During the whole simulation energy can dissipate into a fermion bath, with a flat desity of states as described in 3.3 and the coupling strength $\lambda = 0.5$. Going to a finite U after the system was initially in a zero-temperature anti-ferromagnetic state with $U \to \infty$ corresponds to a strong quench in the Coulomb interaction. The external bath functions not only as a dissipation mechanism so that a steady state can emerge, it also fixes the temperature of the system.

Looking at the spectral function without driving 4.3.1 shows an upper and lower Hubbard band for high temperatures and the formation of low frequency excitations for $T \leq 0.2$, an indicator for Kondo physics. We can estimate the Kondo temperature over the formula $k_B T_K = U\sqrt{\frac{\Gamma}{2U}} \exp^{-\frac{\pi U}{8\Gamma} + \frac{\pi\Gamma}{2U}}$, which results in $k_B T_K = 0.16$. Increasing the amplitude of the driving field effectively increases the temperature and therefore leads to the destruction of the Kondo peak. A resonant driving field pumps electrons/holes between the lower/upper Hubbard band and accelerates the equilibration of the system, for $A = 1.0$ the

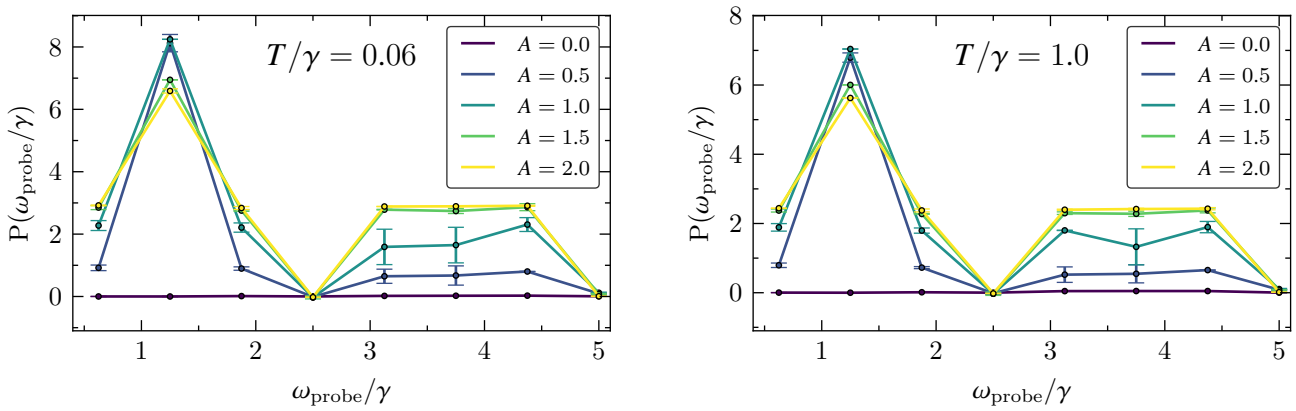

Figure 5: Linear response at resonant pumping for temperatures $T/\gamma = 0.06$ and $T/\gamma = 1.0$

spectral functions are all symmetric and temperature independent except the leftovers of a small Kondo peak.

Probing at a frequency corresponding to the energy difference between th side bands and the Kondo peak ($\omega_{probe} = 2.5$) shows a small response for $A = 0$ and goes to negative values for $A \geq 0.5$, which can be interpreted as an energy flow from the bath into the system. Probing at the same frequency as we are pumping shows that the response first increases as we would expect from the evolution of the spectral functions 4.3.1. This trend changes at the treshold value of $A = 1.0$ and the response starts to decrease again until the response of the highest pump amplitude reaches the same scale as the response without a driving field.

It is also surprising that there is almost no temperature dependance seen in the response functions, especially for small pump amplitudes. Obviously the response carries information, which is not contained in the single-particle Greens functions we are calculating.

- spin averaged and time evolved spectral functions

Half-resonant driving at intermediate U

We are doing the same analysis for a pump frequency of half the bandgap.

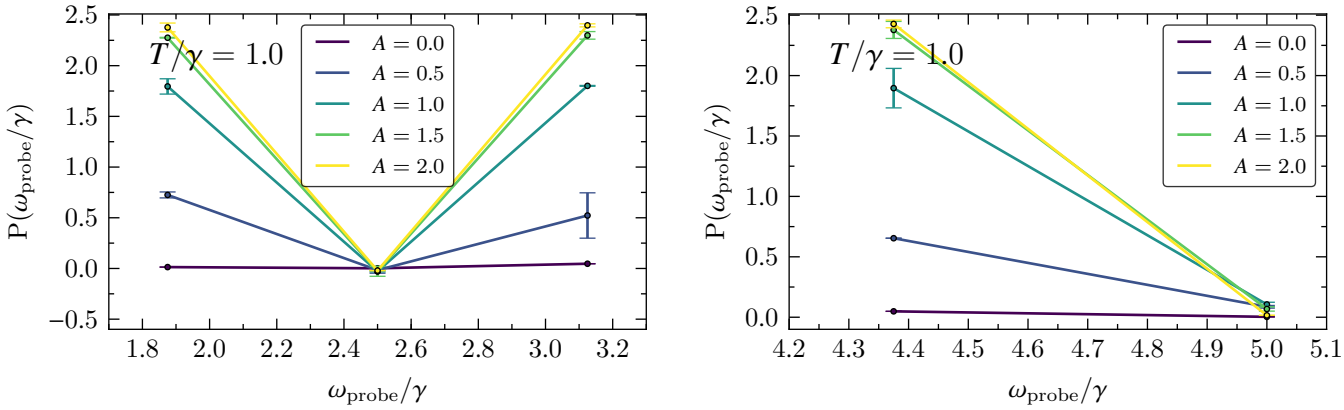

Figure 6: Zoom into $\omega_{probe} = 2.5$ and $\omega_{probe} = 5.0$

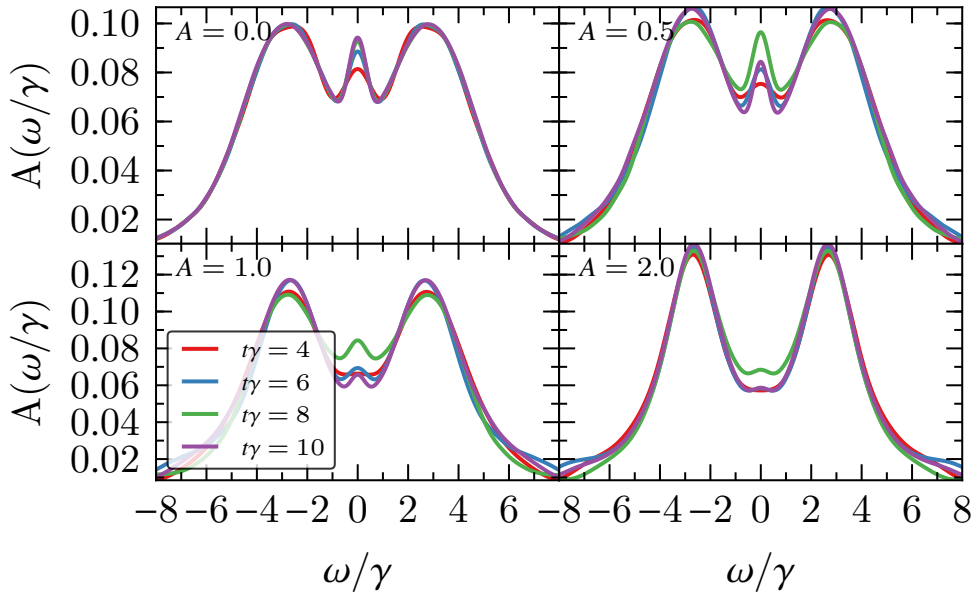

Figure 7: Time-evolved spectral functions, averaged over the initial spin-up and spin-down state at different temperatures. An electric field ($\omega_{pump} = 5$) with increasing strength is applied.

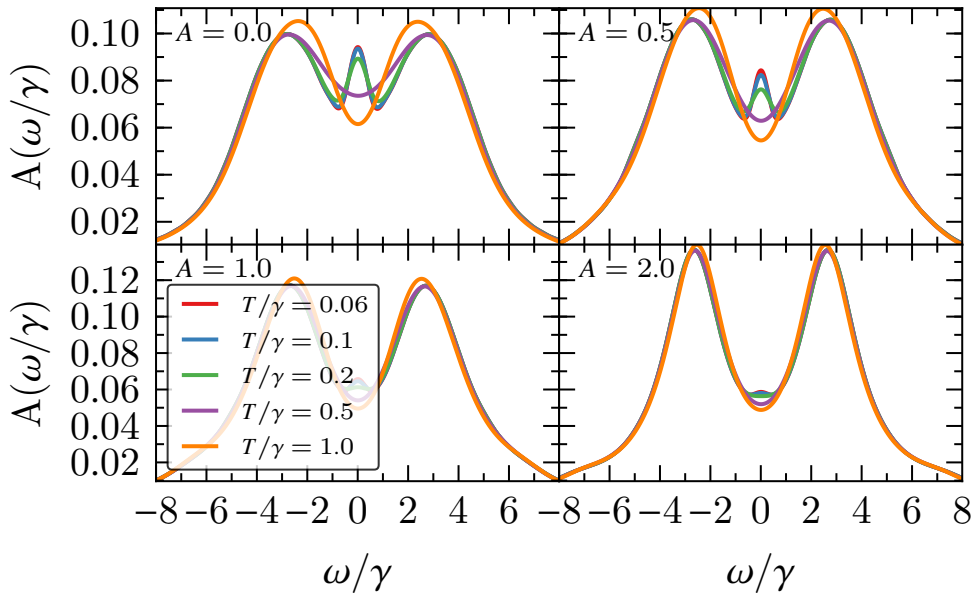

Figure 8: Spectral function averaged over an initial spin up and spin down dot state for different temperatures and various pump amplitudes at resonant driving.

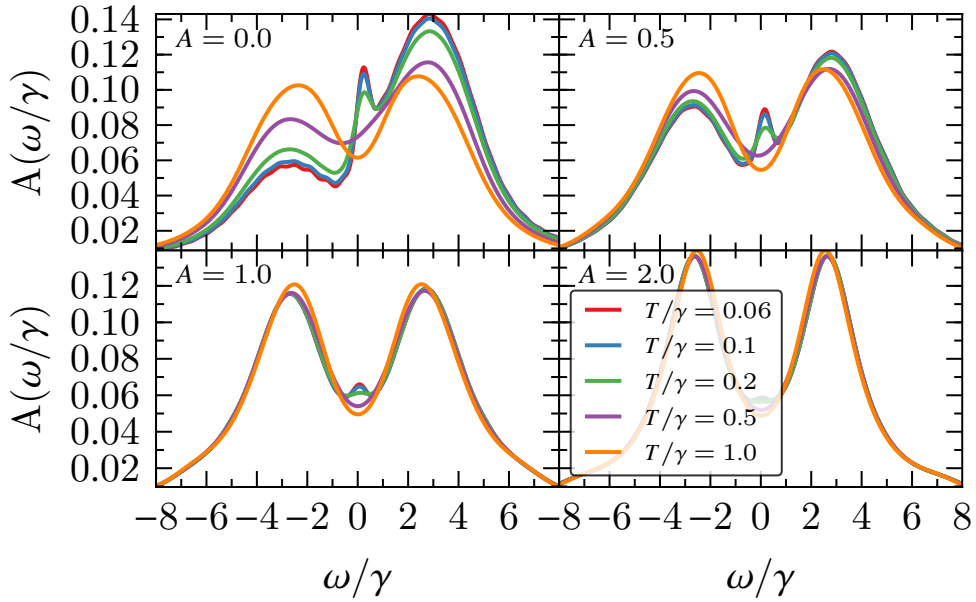

Figure 9: Spectral functions for an initial spin-up state for different temperatures and pump amplitudes at resonant driving.

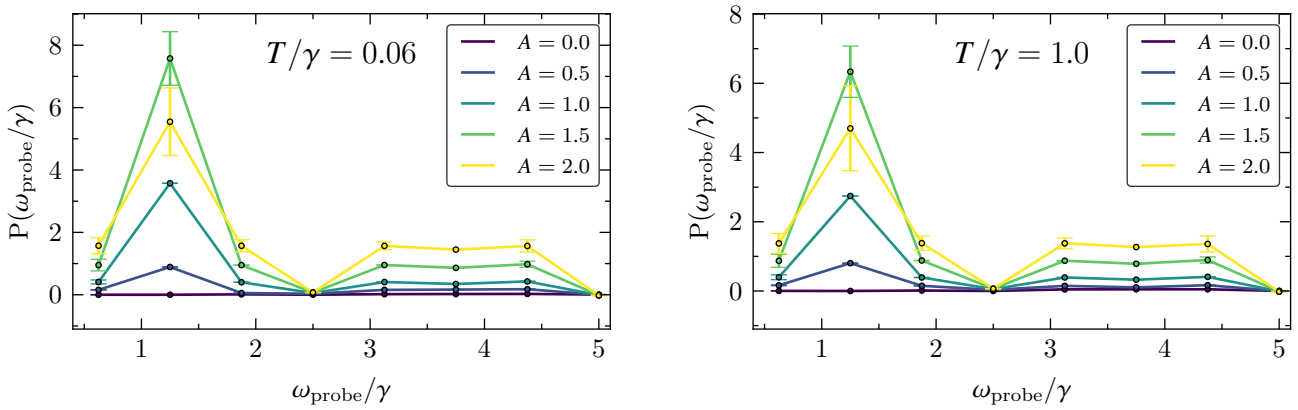

Figure 10: Linear response at half-resonant pumping for temperatures $T/\gamma = 0.06$ and $T/\gamma = 1.0$

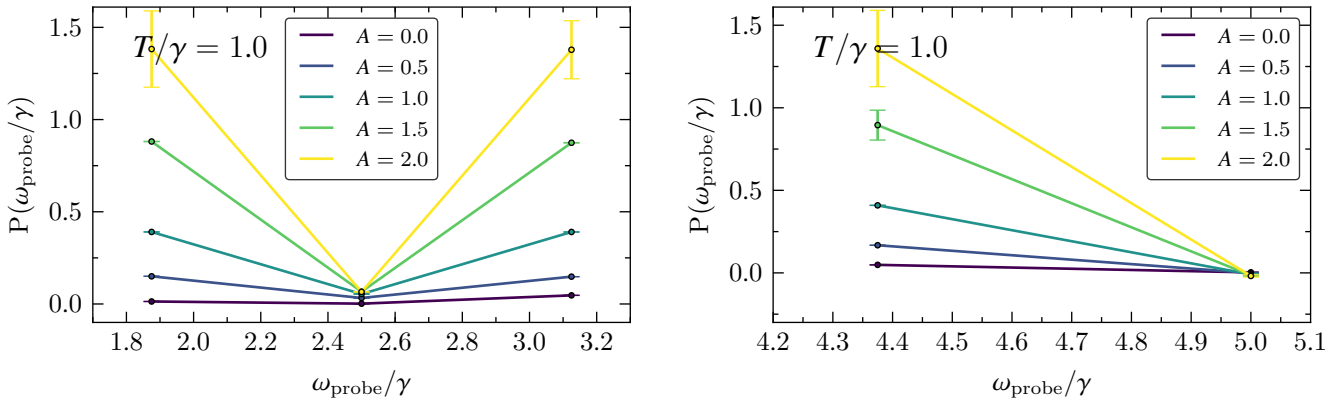

Figure 11: Zoom into $\omega_{probe} = 2.5$ and $\omega_{probe} = 5.0$

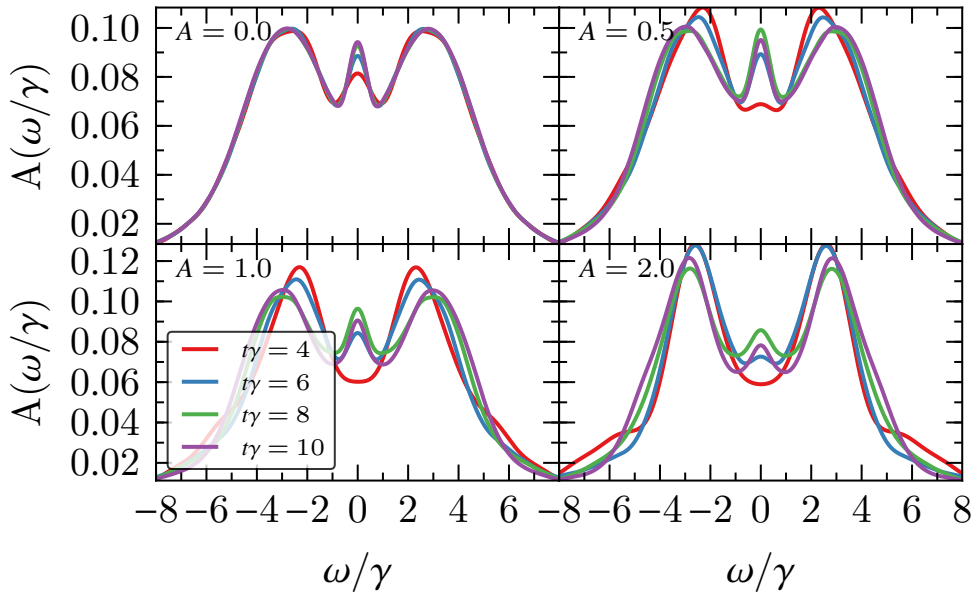

Figure 12: Time-evolved spectral functions, averaged over the initial spin-up and spin-down state at different temperatures. A half-resonant electric field ($\omega_{pump} = 2.5$) with increasing strength is applied.

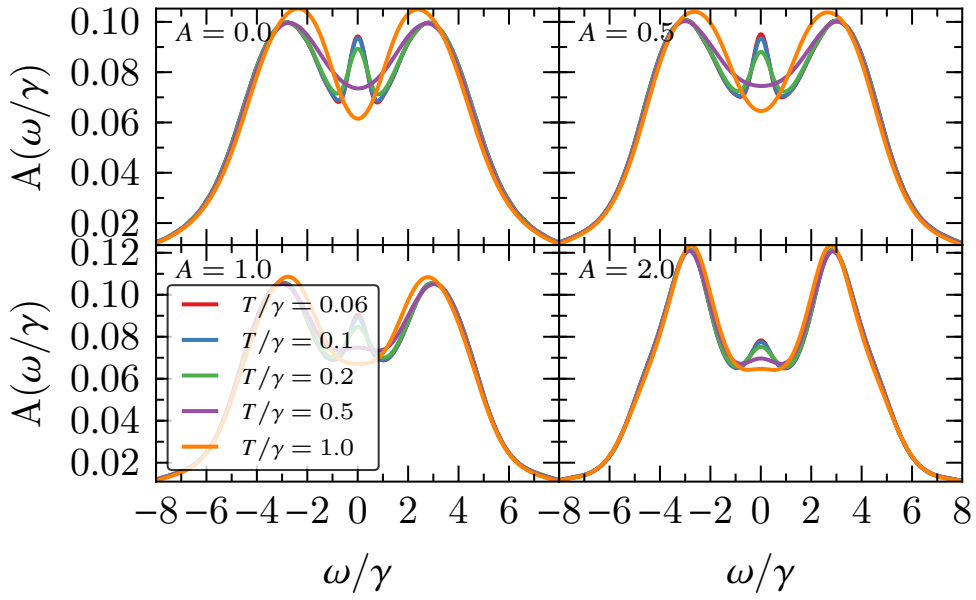

Figure 13: Spectral function averaged over an initial spin up and spin down dot state for different temperatures and various pump amplitudes at half-resonant driving.

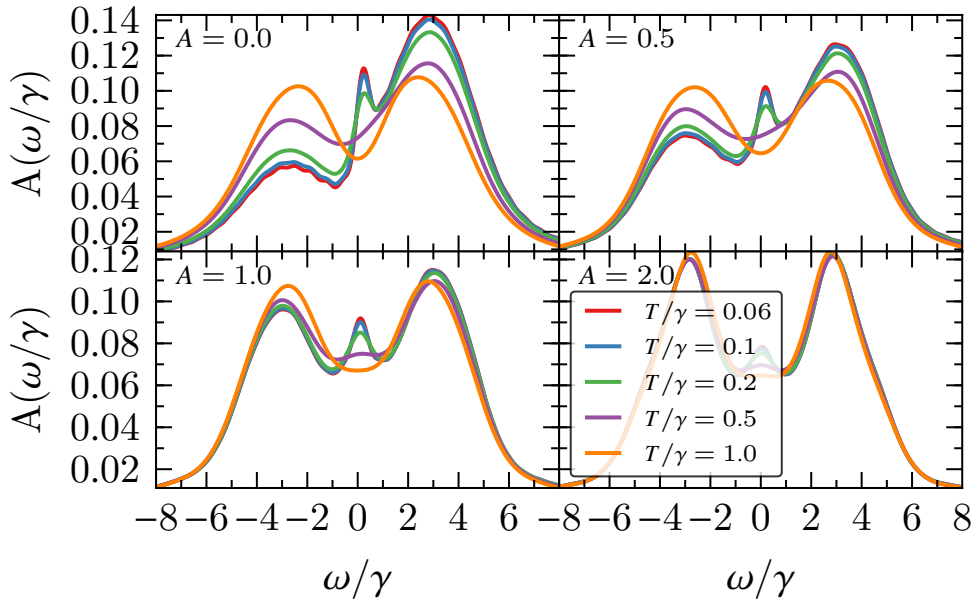

Figure 14: Spectral functions for an initial spin-up state for different temperatures and pump amplitudes at half-resonant driving.

Resonant driving at high U

Half-resonant driving at high U

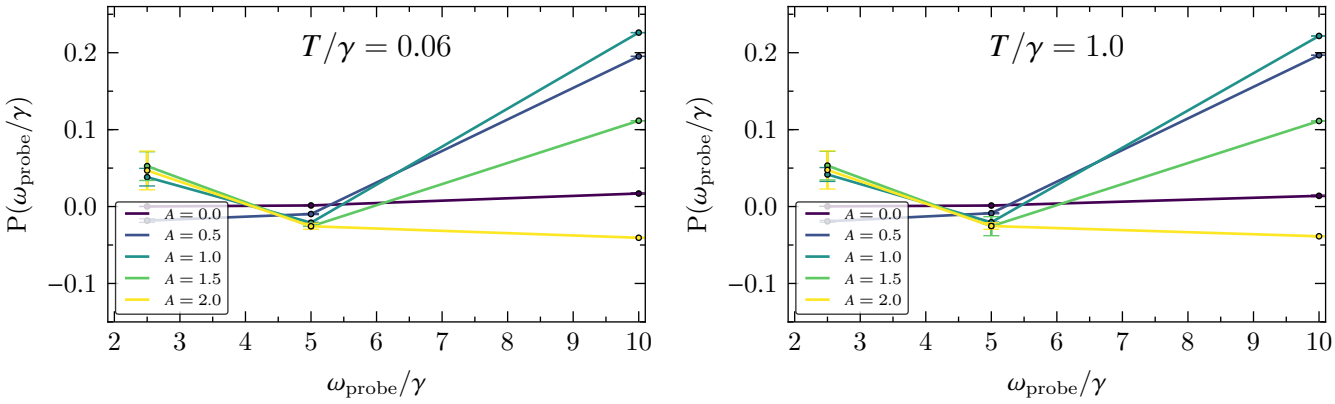

Figure 15: Linear response at resonant driving ($\omega_{pump} = 10$) for temperatures $T/\gamma = 0.06$ and $T/\gamma = 1.0$

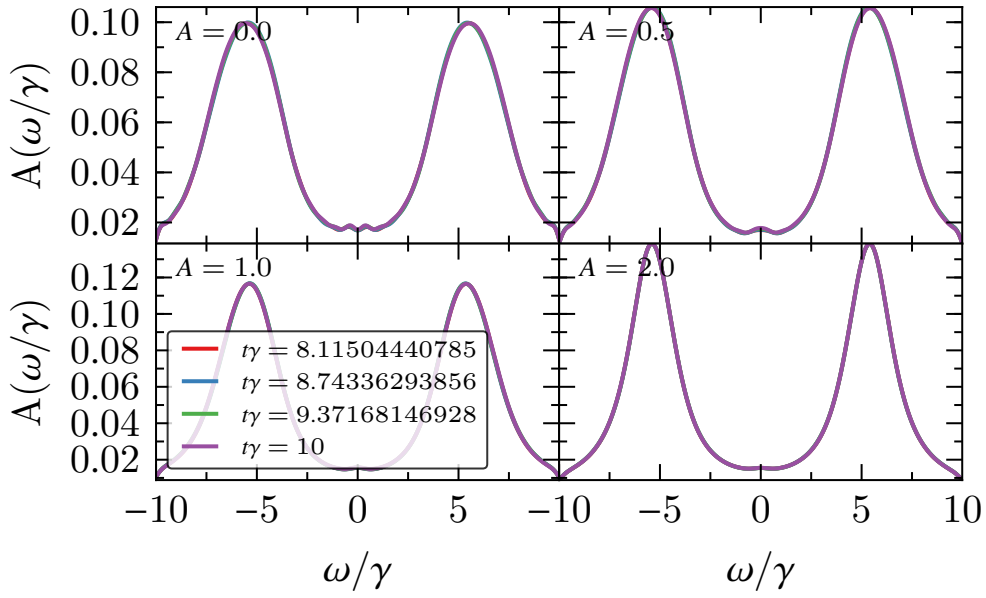

Figure 16: Time-evolved spectral functions, averaged over the initial spin-up and spin-down state at different temperatures. A resonant electric field with increasing strength is applied.

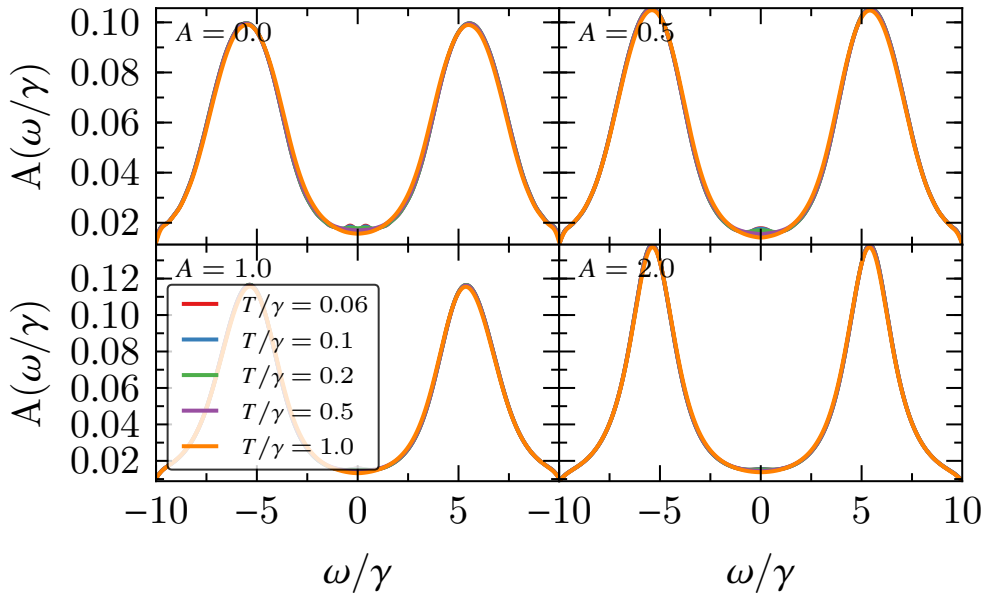

Figure 17: Spectral function averaged over an initial spin up and spin down dot state for different temperatures and various pump amplitudes at resonant driving.

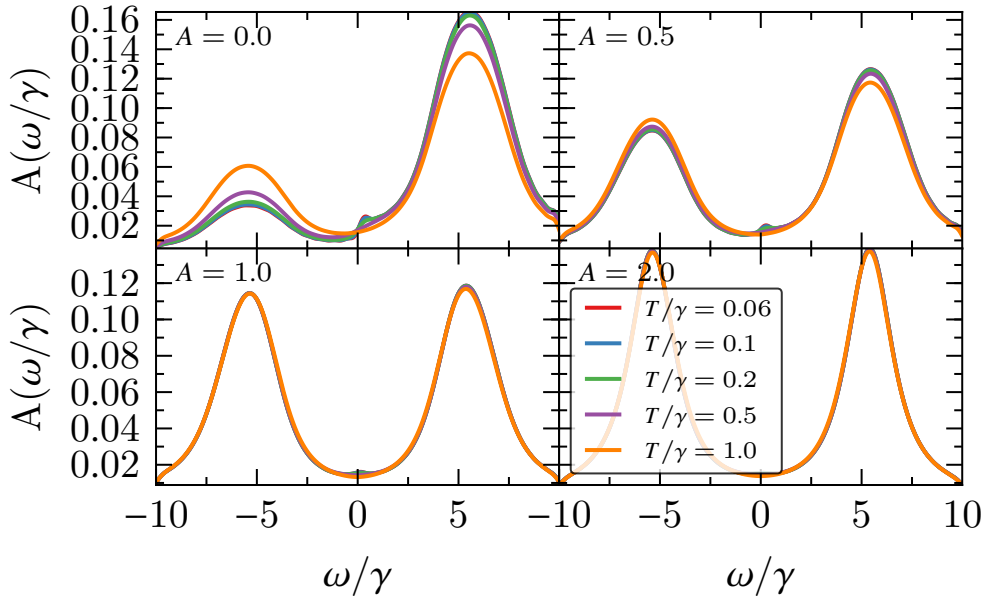

Figure 18: Spectral functions for an initial spin-up state for different temperatures and pump amplitudes at resonant driving.

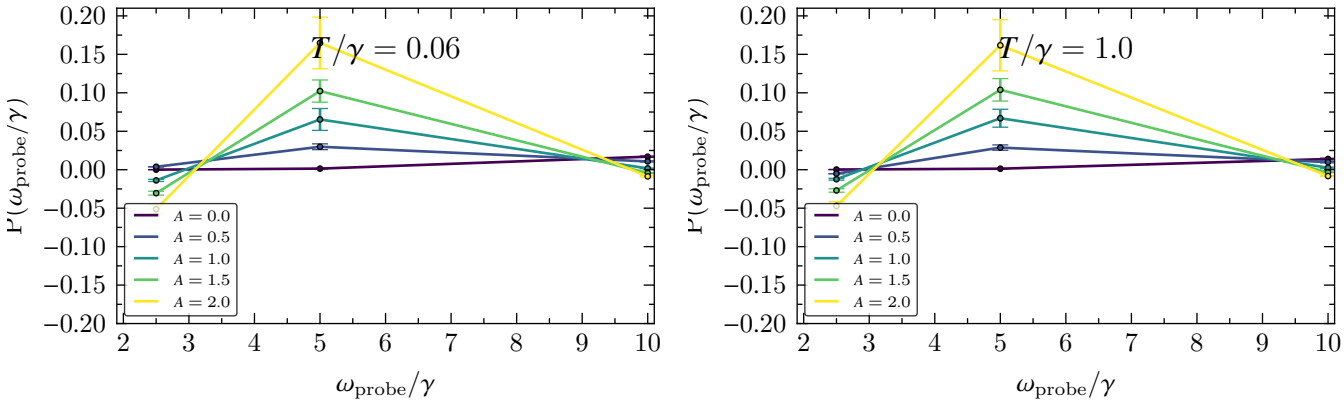

Figure 19: Linear response at half-resonant pumping for temperatures $T/\gamma = 0.06$ and $T/\gamma = 1.0$

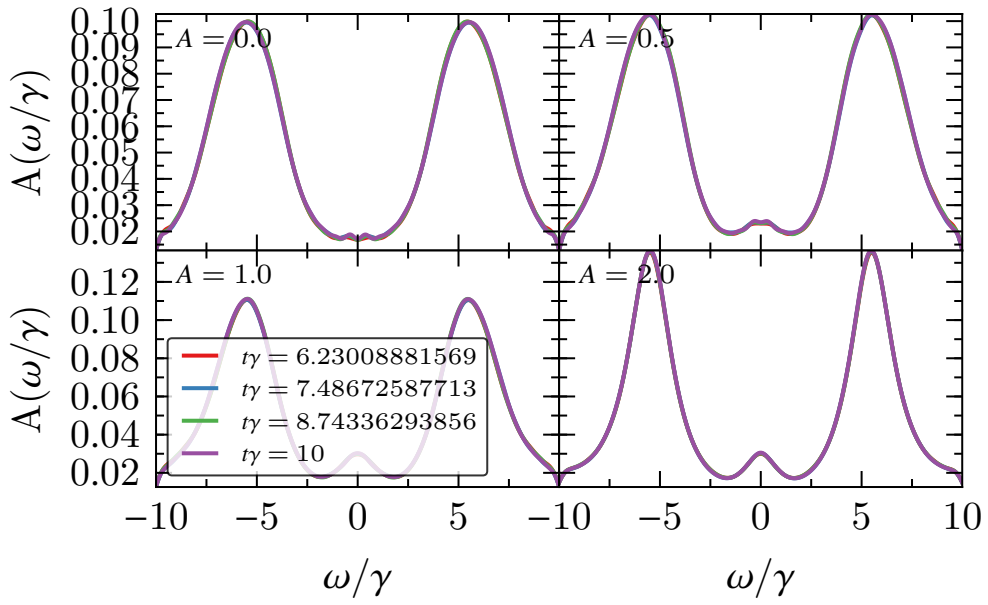

Figure 20: Time-evolved spectral functions, averaged over the initial spin-up and spin-down state at different temperatures. An electric field ($\omega_{pump} = 5$) with increasing strength is applied.

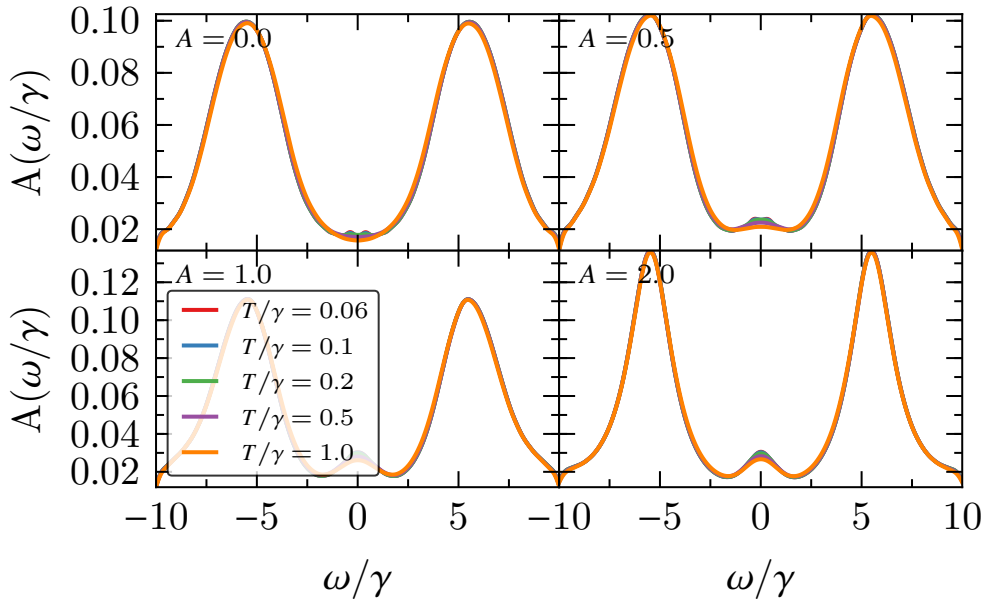

Figure 21: Spectral function averaged over an initial spin up and spin down dot state for different temperatures and various pump amplitudes at resonant driving.

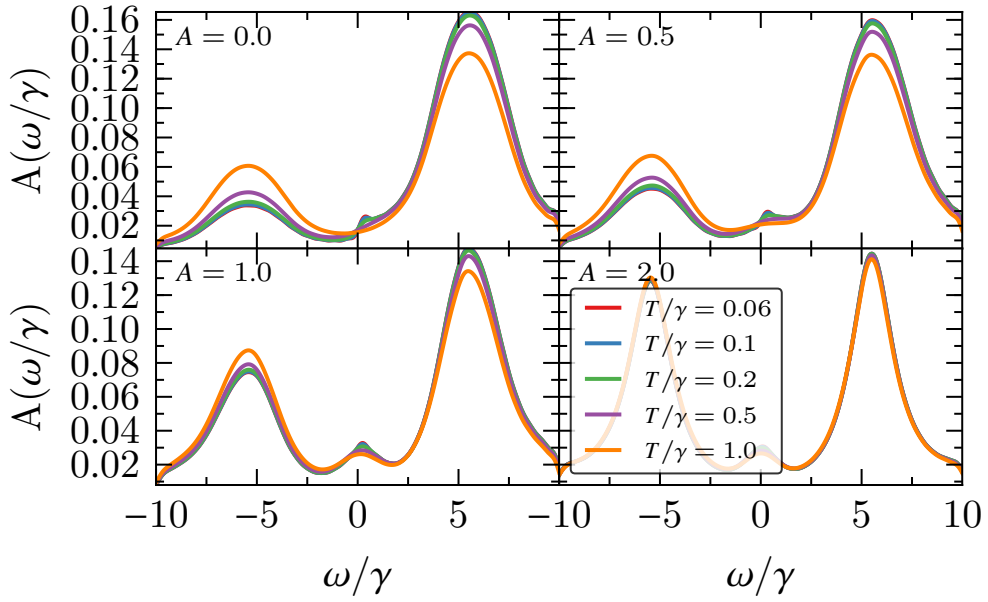

Figure 22: Spectral functions for an initial spin-up state for different temperatures and pump amplitudes at resonant driving.

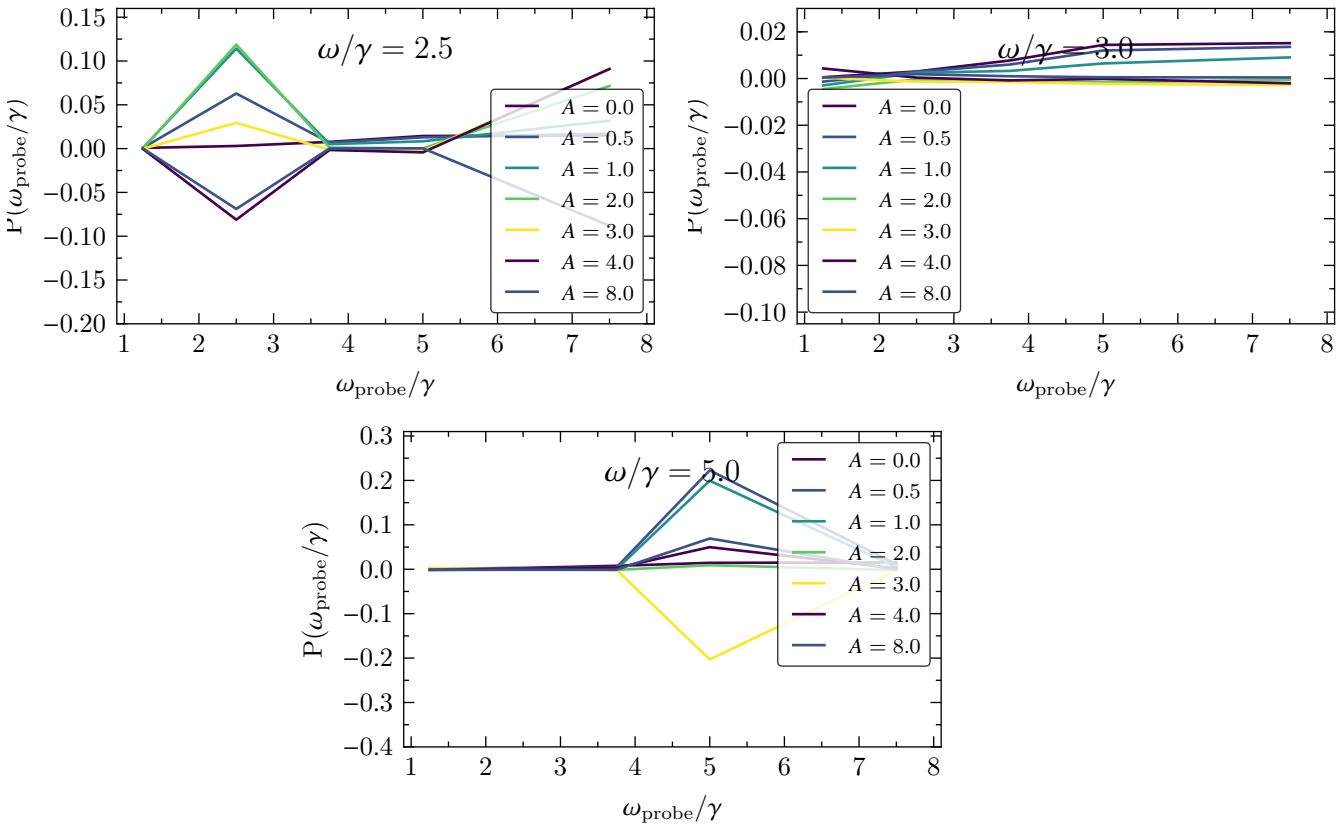

Figure 23: Linear response at different driving frequencies at $T/\gamma = 1.0$

4.3.2 Physical lattice structure

References

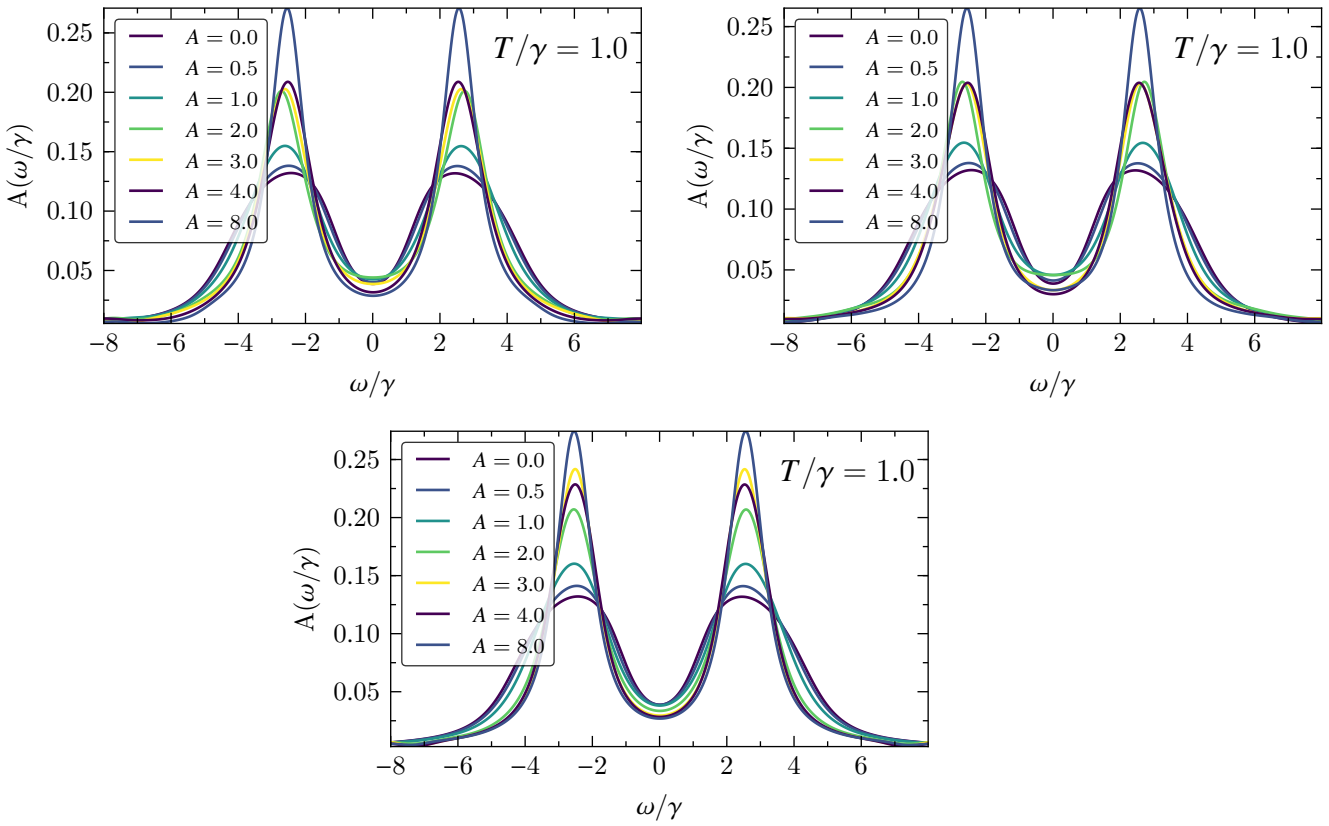

Figure 24: Spectral functions, averaged over the initial spin-up and spin-down state at different electric fields with increasing strength.